Imaging of Pediatric Orbital Diseases

Behroze A. Vachha, MD, PhD[a], Caroline D. Robson, MB,ChB[b,*]

KEYWORDS

• Pediatric • Orbit • Ocular • CT • MR imaging • Congenital • Tumor • Vascular

KEY POINTS

- Orbital diseases in children differ from those found in adults in terms of histopathologic and imaging characteristics.
- Clinical signs are often nonspecific, and imaging is a critical step in evaluating the pediatric orbit, optic pathway, and cranial nerves that supply the orbital contents.
- High-resolution 3-T MR imaging helps characterize orbital and ocular soft-tissue lesions, permitting superior delineation of orbital soft tissues, cranial nerves, blood vessels, and blood flow and detection of intracranial extension of orbital disease.
- Computed tomography (CT) is reserved primarily for evaluation of orbital bony architecture.

INTRODUCTION

The wide spectrum of orbital disease seen in children differs substantially from that found in adults in terms of histopathologic and imaging features. Clinical symptoms and signs such as proptosis, strabismus, diplopia, and optic disc edema are nonspecific, and diagnostic imaging studies play an essential role in depicting the nature and extent of orbital abnormalities, often providing a definitive diagnosis or a relevant differential diagnosis. The information provided by imaging is also important in determining optimal medical or surgical treatment and assessing response to treatment. In this article, the salient clinical and imaging features of various pediatric orbital lesions are described, and the differential diagnoses are reviewed.

NORMAL ANATOMY

The orbital contents are contained within a bony pyramid. The orbital roof is formed by the orbital plate of the frontal bone. The lateral wall is formed by the orbital surface of the zygomatic bone and greater wing of the sphenoid. The frontal process of the maxillary bone, the lacrimal bone, lamina papyracea of the ethmoid bone, and the lesser wing of the sphenoid make up the medial wall from anterior to posterior. The orbital floor is formed by the orbital surfaces of the zygomatic, maxillary, and palatine bones. The optic foramen forms the apex of the bony pyramid and is formed by the lesser wing of the sphenoid. The superior orbital fissure is limited by the lesser wing of the sphenoid superomedially and the greater wing of the sphenoid inferolaterally. The inferior orbital fissure lies between the orbital floor and the greater wing of the sphenoid. The optic canal and superior and inferior orbital fissures transmit nerves and vessels (**Table 1**); spread of tumor along these conduits can occur from the orbit to extraorbital compartments including intracranial extension.

The orbital contents are divided into the intraocular compartment or globe, the muscle cone, and

Disclosures: None.

[a] Department of Radiology, Massachusetts General Hospital, 55 Fruit Street, Boston, MA 02114, USA; [b] Department of Radiology, Boston Children's Hospital, Harvard Medical School, 300 Longwood Avenue, Boston, MA 02115, USA

* Corresponding author.

E-mail address: caroline.robson@childrens.harvard.edu

Neuroimag Clin N Am 25 (2015) 477–501

http://dx.doi.org/10.1016/j.nic.2015.05.009

1052-5149/15/$ – see front matter

Table 1
Contents of orbital foramina

Foramen	Contents
Superior orbital fissure	Cranial nerves III, IV, V_1, VI Superior ophthalmic vein Orbital branch of middle meningeal artery
Inferior orbital fissure	Cranial nerve V_2 Infraorbital vein Infraorbital artery
Optic canal	Cranial nerve II Ophthalmic artery

the intraconal and extraconal spaces (Fig. 1A). The extraocular muscles include the superior, inferior, medial, and lateral rectus muscles and the superior and inferior obliques; all but the inferior oblique muscles constitute the muscle cone (see Fig. 1B). The levator palpebrae superioris lies superior to the superior oblique muscle. The extraocular muscles converge at the orbital apex to form a fibrous connective tissue ring known as the annulus of Zinn. The nonocular compartment of the eye is divided by the muscle cone into conal (muscle cone and annulus of Zinn), intraconal, and extraconal spaces. The intraconal space contains fat, the ciliary ganglion, the ophthalmic artery and vein, and branches of the ophthalmic nerve. The ophthalmic artery and vein and cranial nerves enter the intraconal space through the annulus of Zinn. The extraconal space contains fat, the lacrimal gland, and cranial nerves (branches of the ophthalmic and trochlear nerves). The superior oblique muscles receive motor supply from the trochlear nerves (cranial nerve IV). The lateral rectus muscles are innervated by the abducens

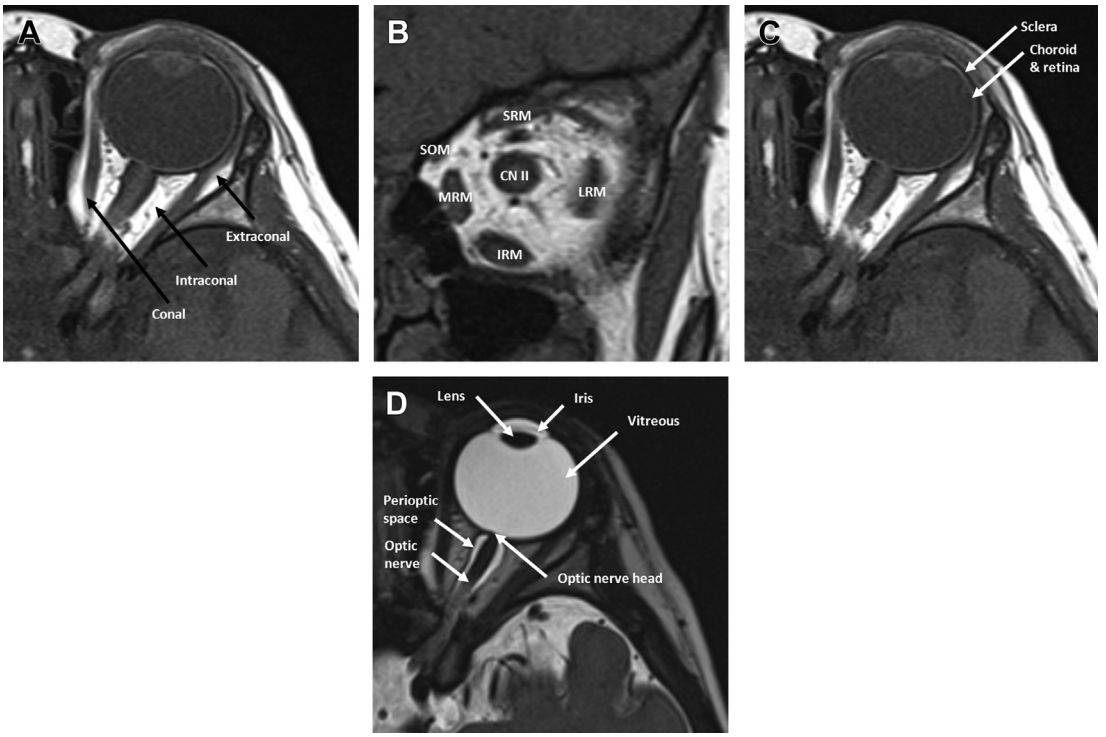

Fig. 1. Normal orbital anatomy. (*A*) High-resolution T1-weighted MR image shows the orbit divided into intraconal and extraconal spaces by the muscle cone and their relationships to the globe. (*B*) Coronal high-resolution T1-weighted MR image of the orbit shows the configuration of the extraocular muscles and the optic nerve. (*C*) High-resolution axial T1-weighted MR image and (*D*) axial T2 sampling perfection with application optimized contrasts using different flip angle evolution (SPACE) MR image showing ocular anatomy. The sclera is hypointense and continuous anteriorly with the cornea and posteriorly with dura. Normal choroid and retina are not distinguishable from each other and appear as an intermediate-intensity structure deep to the sclera on the T1-weighted image. The choroid is continuous anteriorly with the iris and ciliary body, and together, these structures make up the uvea. The lens appears hypointense on the T2-weighted image. Anterior to the lens is a faintly visible linear hypointensity, which is the iris. The iris separates the anterior segment into anterior and posterior chambers containing aqueous humor. The posterior segment lies posterior to the lens and contains the gelatinous vitreous. CN II, cranial nerve II (optic nerve); IRM, inferior rectus muscle; LRM, lateral rectus muscle; MRM, medial rectus muscle; SOM, superior oblique muscle; SRM, superior rectus muscle.

nerves (cranial nerve VI), and the oculomotor nerves (cranial nerve III) supply motor function to the remaining extraocular muscles.

The globe consists of 3 distinct layers from the outside to inside: sclera, uvea, and retina (see Fig. 1C, D). The choroid and retina are inseparable on routine cross-sectional imaging but can be differentiated in the presence of choroidal or retinal detachments. The uvea consists of the iris, ciliary body, and choroid (the most vascular structure of the globe). The retina continues posteriorly as the optic nerve. The collagenous sclera is continuous anteriorly with the cornea and posteriorly with the dura and appears hypointense on T1-weighted MR images at 3T (see Fig. 1C).

IMAGING TECHNIQUE

Imaging of the orbit is primarily accomplished by ultrasonography (US) (evaluation of the globe), CT (bony anatomy), and MR imaging (soft-tissue characterization). CT is indicated for the bony assessment in craniofacial anomalies, trauma, orbital complications of acute sinusitis (with contrast), and assessment of bony remodeling or destruction from orbital masses. Helical 2.5- to 3-mm axial images are obtained with multiplanar soft-tissue and submillimeter bone reformats. CT angiography (CTA) may be obtained for diagnosis or follow-up of suspected orbital arteriovenous malformation (AVM) or arteriovenous fistula (AVF). The parameters for CT should use the lowest dose possible while still providing diagnostic quality images.

Orbital MR imaging is optimally achieved at 3T using a 32-channel phased-array head coil or equivalent coil when possible. In some instances specialized orbital surface coils may be used. Imaging protocols depend on clinical indications. For example, suspected tumors are imaged with high-resolution, thin-section (<3 mm) axial and coronal fat-suppressed T2; axial non-echo planar diffusion-weighted imaging (DWI); axial T1 and multiplanar high-resolution, fat-suppressed, gadolinium-enhanced T1-weighted images. MR venography (MRV) and/or MR angiography (MRA) are sometimes indicated for vascular assessment. Heavily T2-weighted 3-dimensional sequences with submillimeter-thick images (eg, sampling perfection with application optimized contrasts using different flip angle evolution [SPACE], constructive interference in steady state [CISS], fast imaging employing steady state acquisition [FIESTA], sensitivity encoding [SENSE]) are of use for ocular assessment, especially for intraocular tumors such as retinoblastoma and for assessment of cranial nerves. Congenital strabismus and eye movement disorders generally require a combination of thin-section high-resolution axial and coronal T1-weighted images for assessment of the size, shape, and position of the extraocular muscles and imaging of the brain and relevant cranial nerves.

Conventional catheter angiography is reserved for the delineation of orbital AVM or AVF and sometimes for endovascular treatment.

CONGENITAL AND DEVELOPMENTAL ANOMALIES

Anophthalmos and Microphthalmos

Anophthalmos or anophthalmia refers to congenital absence of the eyes.[1,2] Anophthalmos and microphthalmos are a significant cause of congenital blindness and can be isolated or syndromic.[2–4] Several genetic mutations involving *PAX6, SOX2*, and *RAX* genes are associated with these conditions.[5]

Primary anophthalmos is bilateral in approximately 75% of cases and occurs because of failure of optic vesicle development at approximately 22 to 27 days of gestation.[6] Secondary anophthalmos is lethal and occurs when the entire anterior neural tube fails to develop. Degenerative or consecutive anophthalmos occurs when the optic vesicles form but subsequently degenerate; consequently neuroectodermal elements may be present in degenerative anophthalmos but are absent in primary and secondary anophthalmos.[7]

Microphthalmos refers to a small ocular globe with an ocular total axial length (TAL) 2 standard deviations less than that of the population age-adjusted mean.[2] Microphthalmos is further classified as severe (TAL <10 mm at birth or <12 mm after 1 year of age), simple, or complex depending on the anatomic appearance of the globe and the degree of TAL reduction.[8] Simple microphthalmos refers to an intact globe with mildly decreased TAL. Complex microphthalmos refers to a globe with anterior segment dysgenesis (developmental abnormalities of the globe anterior to the lens) and/or posterior segment dysgenesis (developmental abnormalities of the globe posterior to the lens) with mild, moderate, or severe decrease in TAL.[8] Severe microphthalmos may be difficult to differentiate from anophthalmia.[1,2] Both severe microphthalmos and degenerative anophthalmos contain neuroectodermal tissues and are considered as entities along a continuum. The diagnosis is usually based on clinical and imaging criteria.

US is used to determine the ocular TAL in microphthalmos. CT and MR imaging demonstrate an absent globe in anophthalmos (Fig. 2). Amorphous tissue with intermediate density on CT, intermediate signal on T1-weighted images, and low signal on T2-weighted MR images may be noted

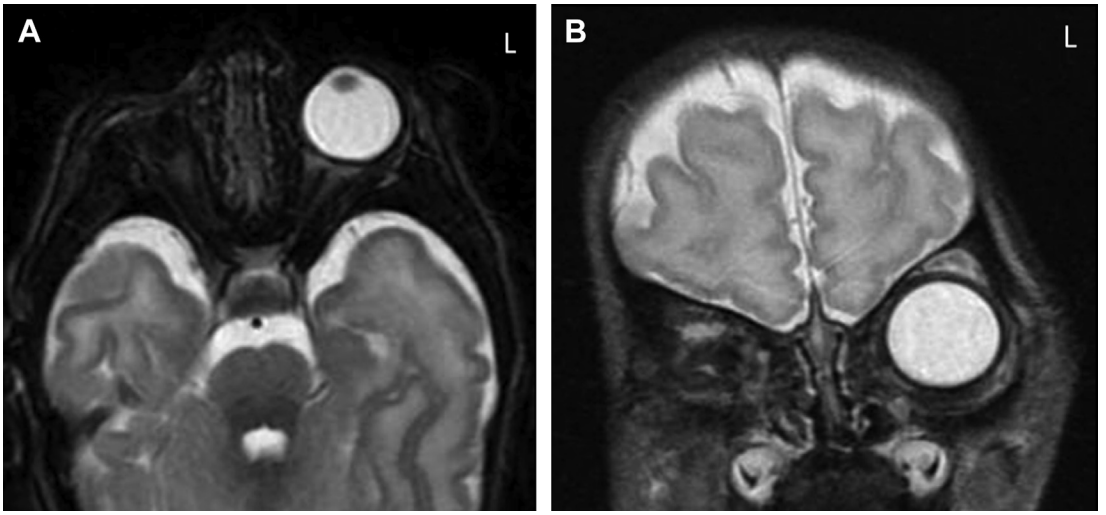

Fig. 2. Unilateral anophthalmos. A 5-day-old baby girl with unilateral right-sided anophthalmos. (*A*) Axial and (*B*) coronal T2-weighted images demonstrate complete absence of the right globe. Note the presence of amorphous tissue and structures resembling extraocular muscles within the anophthalmic right orbit. The right optic nerve is absent.

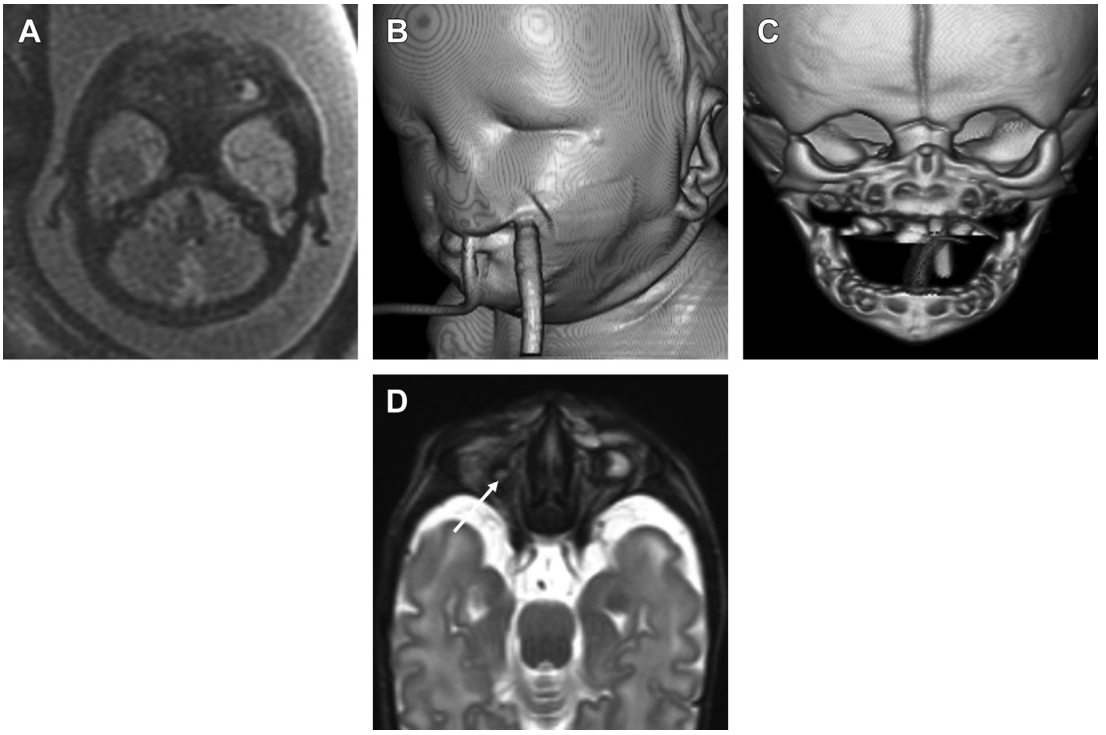

Fig. 3. Severe microphthalmos. Fetus with craniofacial anomalies. (*A*) Fetal MR image at 34 weeks reveals apparent right anophthalmos and left microphthalmos. The fetal nose is absent. (*B*) Postnatal 3-dimensional (3D) CT surface reconstruction image at 3 days of age demonstrates arrhinia and bilateral cryptophthalmos. (*C*) 3D CT image of the skull shows shallow malformed orbits and absence of the nares. (*D*) Axial T2-weighted MR image shows a rudimentary cystic structure within the right orbit (*arrow*), which in retrospect can be seen on the fetal MR image, and left microphthalmos. The infant was diagnosed with Bosma syndrome.

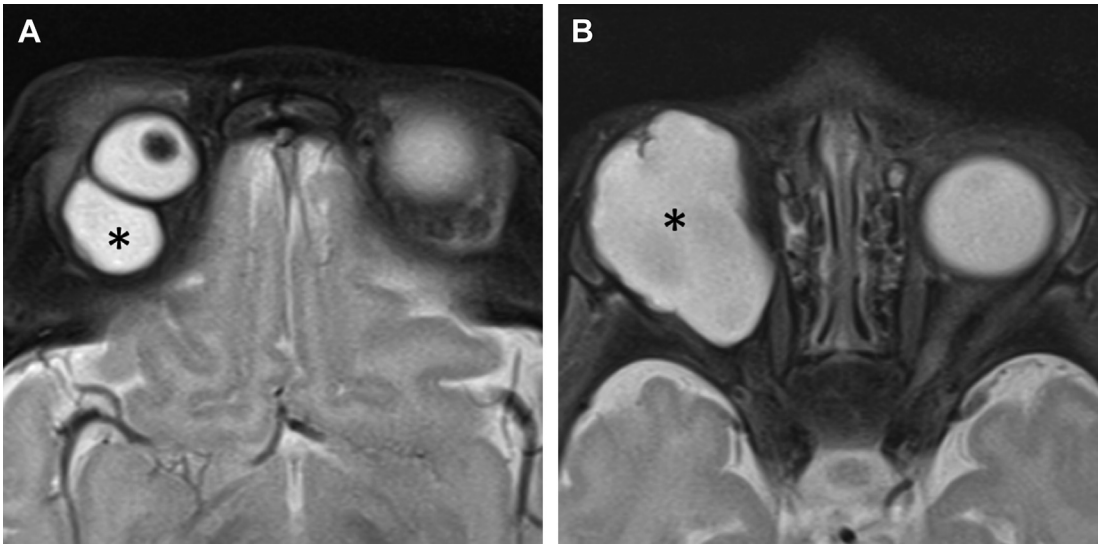

Fig. 4. Unilateral microphthalmos and cyst. A 2-month-old baby girl with persistent closure of the right eye. Clinical examination revealed right microcornea and microphthalmos with bluish discoloration of the lower eyelid thought to represent a cyst. (*A, B*) Axial fat-suppressed T2-weighted MR images confirm microphthalmos associated with a cyst. The globe is small, deformed, and displaced superiorly. The large cyst (*asterisk*) is located posterosuperior to the globe.

particularly in degenerative anophthalmos. Orbital dimensions and volumes are reduced in anophthalmos and usually in microphthalmos, unless associated with an intraorbital cyst (Figs. 3 and 4). Simple microphthalmos demonstrates a normal albeit small globe, with normal signal characteristics.

Mild to moderate microphthalmia is managed conservatively with conformers, whereas severe microphthalmia and anophthalmia are treated with endo-orbital volume replacements (implants, expanders, and dermis-fat grafts) and soft-tissue reconstruction.[2,8]

Cryptophthalmos

Embryologically, the eyelid folds appear during the seventh week and grow toward each other and fuse, with separation of lids occurring between the fifth and seventh months of development.[5,9] Cryptophthalmos is usually syndromic and results from failure of development of the eyelid folds with absence of eyebrows, eyelids, and the cornea and continuous skin extending from the forehead to the cheeks. Imaging is required to demonstrate the status of the underlying ocular globes and orbital structures before surgical intervention (see Fig. 3).

Anterior Segment Dysgenesis

Anterior segment dysgenesis results from faulty development of the anterior ocular structures, including the cornea, iris, ciliary body, lens, and anterior and posterior chambers, resulting in an increased risk of glaucoma and blindness. Anterior segment anomalies are associated with *PITX2, FOXC1 PAX6* and related mutations and produce findings such as aniridia, iris hypoplasia, primary congenital glaucoma, Axenfeld-Rieger syndrome (congenital angle anomalies with iris strands), and Peter anomaly (corneal clouding with adhesions between iris, lens, and cornea).[10] Although many of these anomalies produce ophthalmologic abnormalities that do not require further imaging, thin-section high-resolution T2-weighted 3T MR images may demonstrate abnormal size and shape of the anterior and posterior chambers and/or buphthalmos (Fig. 5).

Macrophthalmos

Elongation of the anteroposterior (AP) diameter of the posterior chamber of the globe is most frequently caused by severe myopia. Buphthalmos refers to diffuse enlargement of the AP diameter of the globe (anterior and posterior chambers) usually due to primary congenital or infantile glaucoma or due to syndromic glaucoma as seen in neurofibromatosis type I (NF-1) and Sturge-Weber syndrome.[5]

Imaging is required to differentiate macrophthalmos from other conditions resulting in enlargement of the globe such as an intraocular mass. In buphthalmos, the globe is generally uniformly enlarged but may occasionally have oval or bizarre configurations.[5] Patients with NF-1 demonstrate proptosis, sphenoid wing dysplasia, and orbital plexiform neurofibromas in addition to buphthalmos (Fig. 6).

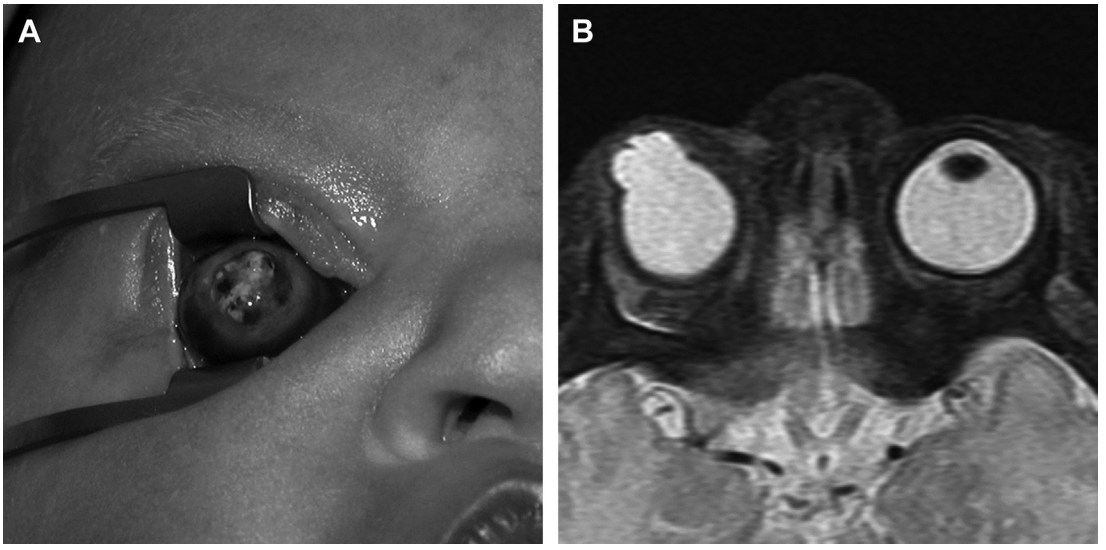

Fig. 5. Anterior segment dysgenesis. (*A*) A 1-day-old baby girl with right proptosis, elevated intraocular pressure, and scleralization with calcification on the anterior surface of the right eye. (*B*) Axial fat-suppressed T2-weighted MR image shows mild right microphthalmos with a large, irregular anterior segment consistent with the clinical finding of anterior segment dysgenesis. There is aniridia and aphakia. Progressive enlargement and exposure of the right eye occurred despite medical therapy. Subsequently, with no potential for visual rehabilitation and risk for perforation, the right eye was enucleated. ([*A*] *Courtesy of* Carolyn Wu, MD, Department of Ophthalmology, Boston Children's Hospital, Boston, MA.)

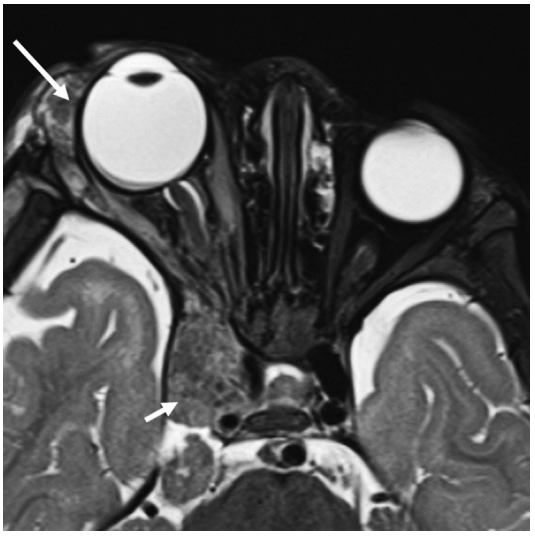

Fig. 6. Macrophthalmia. A 5-month-old girl with NF-1 and proptosis. Axial fat-suppressed T2-weighted MR image reveals enlargement of the right globe, consistent with buphthalmos. There is right sphenoid bone dysplasia with associated enlargement of the right middle cranial fossa. A plexiform neurofibroma is present within the lateral aspect of the orbit (*long arrow*). There is also a nerve sheath tumor within the right cavernous sinus (*short arrow*) and Meckel cave.

Congenital Cystic Eye

Congenital cystic eye is a rare condition resulting from failure of the optic vesicle to invaginate to form the globe. On imaging, a cystic, sometimes septated, orbital mass is seen in place of the normal globe (Fig. 7). The differential diagnosis includes microphthalmia with cyst, microphthalmia with cystic teratoma, ectopic brain tissue, and meningoencephalocele.[11,12]

Coloboma

Coloboma is a developmental anomaly that results from incomplete closure of the embryonic choroidal fissure, resulting in ectasia and herniation of vitreous into the retro-ocular space.[13] The developmental insult occurs during gestational days 35 to 41.[6,7] Colobomas may affect the iris, lens, ciliary body, retina, choroid, sclera, or optic nerve.[14] Colobomas may be unilateral or bilateral and can be isolated or syndromic, as seen in CHARGE syndrome (coloboma, heart defects, choanal atresia, retarded growth and development, genital malformations, and ear anomalies).[12,15] Numerous other genetic disorders are associated with coloboma, including focal dermal hypoplasia, branchio-oculofacial syndrome, trisomies 13 and 18, and Aicardi syndrome.[5]

On MR imaging, coloboma appears as a focal defect of the posterior wall of the globe, sometimes associated with microphthalmia (Fig. 8). A

Fig. 7. Congenital cystic eye. Infant boy on day of birth noted to have a cystic orbital mass at birth. Axial contrast-enhanced CT reveals a large, heterogeneous cystic mass enlarging the orbit. In contrast to other ocular anomalies, no definite ocular structures are seen. At surgical exploration, congenital cystic eye was confirmed with only a small area of pigment consistent with uveal tissue.

minimal defect results in a small excavation along the posterior globe. A larger defect produces a retrobulbar cystic cavity outpouching from the posterior wall of the globe.[12]

Morning Glory Disc Anomaly

Morning glory disc anomaly (MGDA) is a congenital optic nerve anomaly characterized by a funnel-shaped excavation of the optic disc with a central glial tuft overlying the optic disc and an annulus of chorioretinal pigmentary changes surrounding the optic disc excavation.[16–18]

Although MGDA is usually diagnosed clinically, imaging also distinguishes MGDA from optic nerve coloboma. MGDA has 3 distinctive MR imaging findings: (1) funnel-shaped appearance of the optic disc with elevation of the adjacent retinal surface; (2) abnormal tissue associated with the ipsilateral distal intraorbital optic nerve, effacing the adjacent perioptic nerve subarachnoid space; and (3) lack of the usual enhancement at the lamina cribrosa associated with the funnel-shaped defect at the optic papilla (**Fig. 9**).[16] Identification of MGDA at imaging should prompt a search for associated intracranial abnormalities, including midline craniofacial and skull base defects, vascular abnormalities, and cerebral malformations.[19,20] In particular, brain MR imaging and internal carotid artery MRA should be performed because of an association with transphenoidal basal encephalocele and congenital stenoocclusive change of the internal carotid arteries (moyamoya disease) in these patients.[20] MGDA can also be seen in association with PHACES (*p*osterior fossa anomalies, *h*emangioma, *a*rterial and aortic arch anomalies, *c*ardiac anomalies,

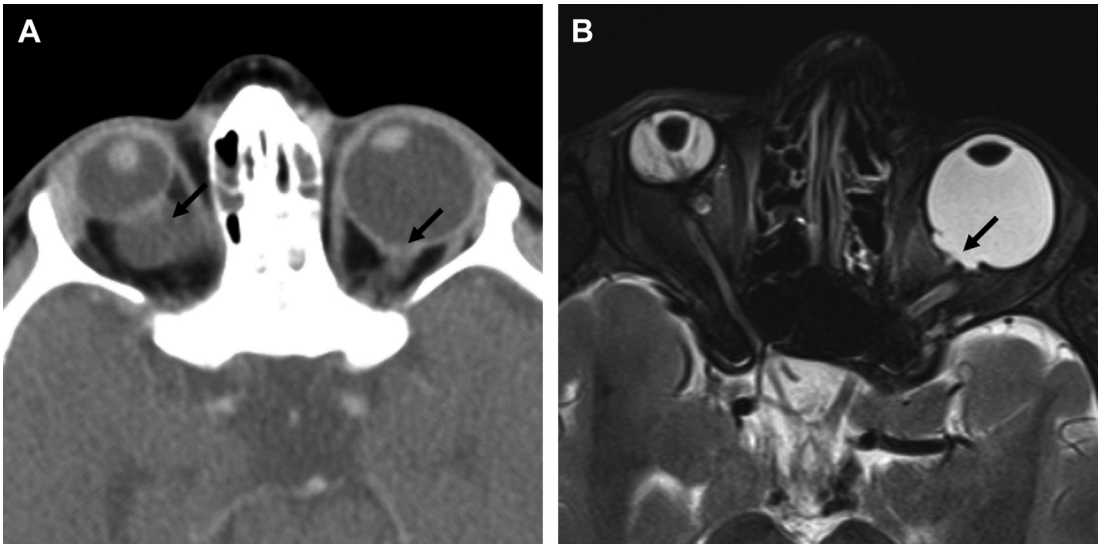

Fig. 8. Coloboma. Girl with CHARGE syndrome, right microphthalmos, and colobomata. (*A*) Axial contrast-enhanced CT obtained at 2 years of age reveals right micropthalmos and bilateral colobomata (*arrows*). (*B*) Axial fat-suppressed T2-weighted MR image at 16 years of age shows an interval right retinal detachment with a small residual cystic structure posterior to the right globe and a large choroidal coloboma involving the left eye (*arrow*).

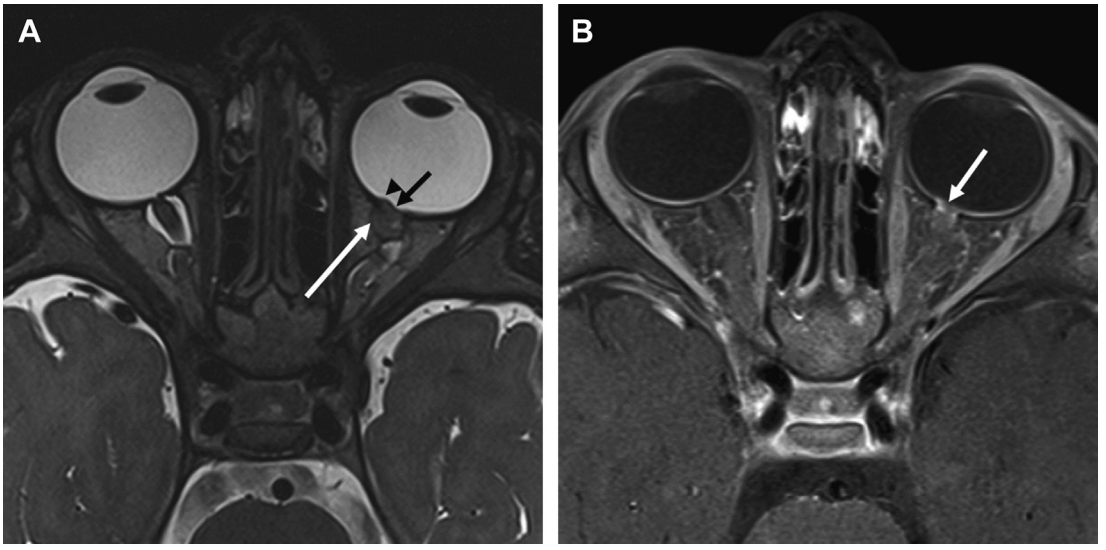

Fig. 9. Morning glory disc anomaly (MGDA). A 21-month-old boy presenting with poor vision and sensory exotropia of the left eye. Ophthalmologic examination revealed a megalopapilla with a central glial tuft and changes consistent with MGDA. (*A*) Axial 3-dimensional T2 SPACE MR image reveals a funnel-shaped appearance of the posterior optic disc (*black arrow*) with elevation of the adjacent retinal surface (*arrowhead*). There is abnormal tissue associated with the distal intraorbital segment of the ipsilateral optic nerve, with effacement of the regional subarachnoid space (*white arrow*). (*B*) Axial fat-suppressed T1-weighted MR image shows discontinuity of enhancement at the lamina cribrosa (*arrrow*), with enhancement extending along the most distal aspect of the optic nerve.

eye anomalies, and sternal anomalies and/or supraumbilical raphe).[21]

Staphyloma

Staphyloma results from thinning and stretching of the uvea and sclera and involves all layers of the globe. Risk factors include severe axial myopia, glaucoma, and severe ocular inflammation. Imaging reveals a posterior outpouching of the globe producing deformity in globe contour (**Fig. 10**).

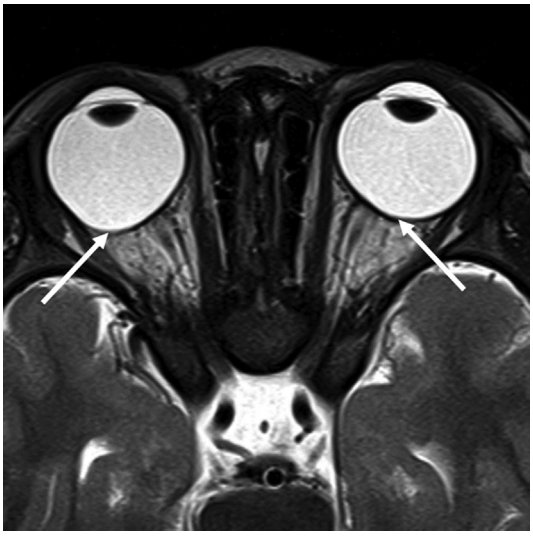

Fig. 10. Staphyloma. A 3-year-old girl with nystagmus, pale optic discs, and esotropia. Axial T2-weighted MR image shows bilateral staphylomas right greater than left. There is smooth outpouching of all layers of the globes along the temporal aspects of the optic nerves bilaterally (*arrows*). The optic nerves appear diminutive in keeping with either optic nerve hypoplasia (congenital) or atrophy (acquired).

Hypertelorism, Hypotelorism, and Cyclopia

Hypertelorism denotes increased distance between the medial orbital walls. Hypertelorism is associated with several craniofacial disorders, including cephaloceles, syndromic agenesis of the corpus callosum, and syndromic coronal craniosynostosis (**Fig. 11**A). Hypertelorism must be distinguished from dystopia canthorum in which the medial orbital walls are normally spaced but the medial intercanthal distance is increased, as seen in various types of Waardenburg syndrome.

Hypotelorism denotes decreased distance between the medial orbital walls. Hypotelorism is also associated with a variety of disorders, including the holoprosencephalies (HPE) and premature fusion of the metopic and sagittal sutures (see **Fig. 11**B). Cyclopia or cyclophthalmia

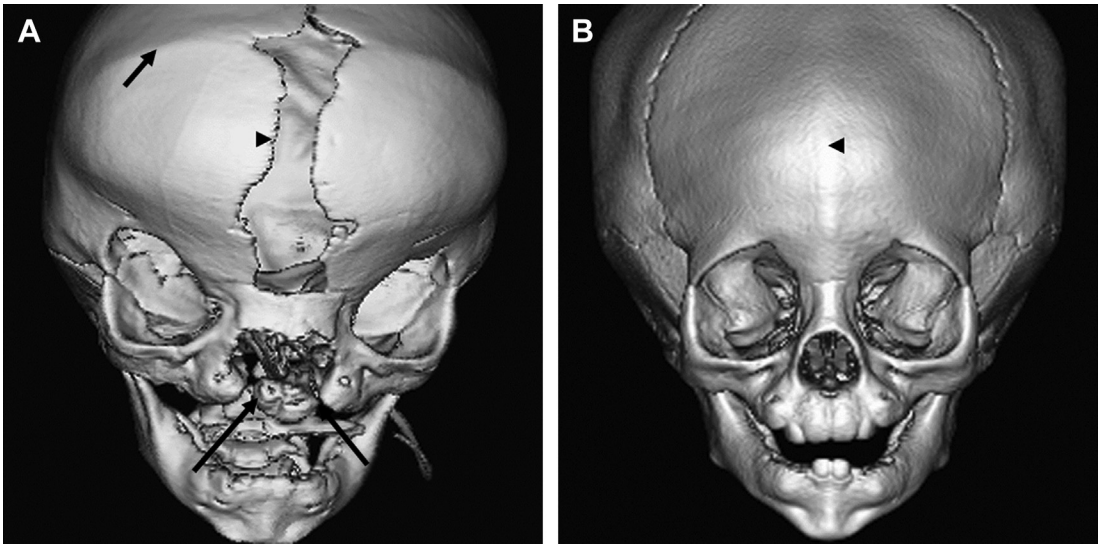

Fig. 11. Hypertelorism and hypotelorism associated with craniosynostosis. (*A*) Three-dimensional (3D) CT image in a 9-month-old girl with brachycephaly and exophthalmos reveals hypertelorism and bilateral cleft lip and palate (*long arrows*). There is bicoronal synostosis (*short arrow*) and wide patency of the metopic suture (*arrowhead*) consistent with the known diagnosis of Apert syndrome. (*B*) 3D CT image in a 7-month-old girl with trigonocephaly shows premature fusion of the metopic suture resulting in frontal ridging (*arrowhead*) associated with hypotelorism.

denotes complete fusion of the optic vesicles resulting in a single median eye. Synophthalmia represents partial fusion of the optic vesicles resulting in duplication of some anterior structures. Both cyclophthalmia and synophthalmia can be associated with HPE.[5] Other manifestations of HPE include ethmocephaly (hypotelorism with median proboscis) and cebocephaly (hypotelorism with rudimentary nose and single nostril).

Large/Small Orbit

A large orbit can be congenital or acquired and results from causes such as cephalocele, bony deformity as seen in NF-1, and bony or orbital masses (see **Figs. 6** and **7**). A small orbit accompanies anopthalmia and microphthalmia (see **Figs. 2** and **3**). Exorbitism denotes shallow orbits as seen in syndromic craniosynostosis (see **Fig. 11**). Exorbitism should not be confused with proptosis in which there is mass effect within the orbit causing ventral protrusion of the globe.

Optic Nerve Hypoplasia

Optic nerve hypoplasia (ONH) is a developmental anomaly characterized by optic nerve underdevelopment. Bilateral ONH is associated with syndromic disorders such as septo-optic dysplasia. On imaging, the affected optic nerves and part or all of the optic chiasm and tracts appear small (see **Fig. 10**). The differential diagnosis for optic hypoplasia is optic atrophy resulting from a variety of causes such as prior infection/inflammation, trauma, irradiation, retinopathy of prematurity (ROP), and vascular insult.

Persistent Hyperplastic Primary Vitreous

Persistent hyperplastic primary vitreous (PHPV) results from failure of the embryonic hyaloid vasculature to involute, resulting in persistence of hyperplastic primary vitreous and the capillary vascular network covering parts of the lens. PHPV is typically unilateral and results in congenital microphthalmos, leukocoria, and cataract. Bilateral PHPV is associated with congenital conditions such as Norrie disease and Warburg disease.[22]

The appearance of PHPV has been likened to that of a martini glass with the glass represented by triangular retrolental fibrovascular tissue and the martini glass stem represented by the stalk of hyaloid remnant extending to the optic disc in Cloquet canal (**Fig. 12**).[23] On CT, PHPV appears as increased density of the vitreous with a V-shaped or linear structure presumed to represent a remnant of the Cloquet canal. On MR imaging, the retrolental fibrovascular tissue and stalklike hyaloid remnant are hypointense on T1- and T2-weighted images with contrast enhancement. Hemorrhage and layering vitreous debris may be seen on imaging. Absence of calcification on CT is an important distinction from retinoblastoma (**Box 1**).

Fig. 12. PHPV. A 1-year-old girl with esotropia, nystagmus, and bilateral chorioretinal colobomas. Axial 3-dimensional T2 SPACE MR image shows a triangular deformity at the posterior aspect of the left lens (*black arrow*) that is contiguous with a linear hypointensity extending toward the optic disc representing the stalk of hyaloid remnant of the Cloquet canal (*arrowhead*). There are also bilateral chorioretinal colobomas (*white arrows*).

Coats Disease

Coats disease is a sporadic disorder characterized by a defect in retinal vascular development resulting in telangiectactic retinal vessels with vessel leakage, subretinal exudate, and retinal detachment.[22,24] Coats disease is unilateral in 80% to 90% of cases, with a male predilection. Common signs are leukocoria and strabismus.[22,24] On CT, Coats disease appears as a hyperdense exudate, typically without calcification (Fig. 13). On MR imaging, the lipoproteinaceous subretinal exudate appears hyperintense on T1- and T2-weighted images. The absence of an enhancing mass helps differentiate Coats disease from retinoblastoma (see Box 1).

Retinopathy of Prematurity

ROP or retrolental fibroplasia is a postnatal fibrovascular organization of the vitreous humor that may lead to retinal detachment. ROP is related to excessive oxygen therapy in premature, low-birth-weight infants but is now uncommon because of therapeutic advances. ROP is bilateral and asymmetric.

ROP presents with microphthalmia and a shallow anterior chamber on CT and MR imaging. On CT, there is hyperattenuation within the globe. Dystrophic calcifications are not typically a feature of ROP until late in the disease (Fig. 14A). The association of dystrophic calcifications with microphthalmia distinguishes ROP from retinoblastoma, in which there is a calcified mass or masses in a normal-sized globe (see Box 1). On MR imaging, there may be hyperintensity within the globe on T1- and T2-weighted imaging due to subretinal

Box 1
Differential diagnosis of leukocoria

Normal-sized eye

Calcified mass

- Retinoblastoma (single or multiple enhancing lesions, grows into vitreous or choroid)

Noncalcified mass

- Coats disease (no enhancing mass, lipoproteinaceous hyperintense subretinal exudate)

Microphthalmia

Unilateral

- PHPV (subhyaloid or subretinal blood-fluid levels, retrolental tubular mass along the hyaloid canal that enhances)

Bilateral

- ROP (no or minimal enhancement, dystrophic calcification late in disease)
- Bilateral PHPV (see earlier)

Fig. 13. Coats disease. A 3-year-old boy with decreased vision left eye. On examination, there was funnel-shaped retinal detachment and neovascular glaucoma consistent with Coats disease of the left eye. Axial CT image shows the V-shaped left retinal detachment (*arrow*). No mass lesion or calcification is seen.

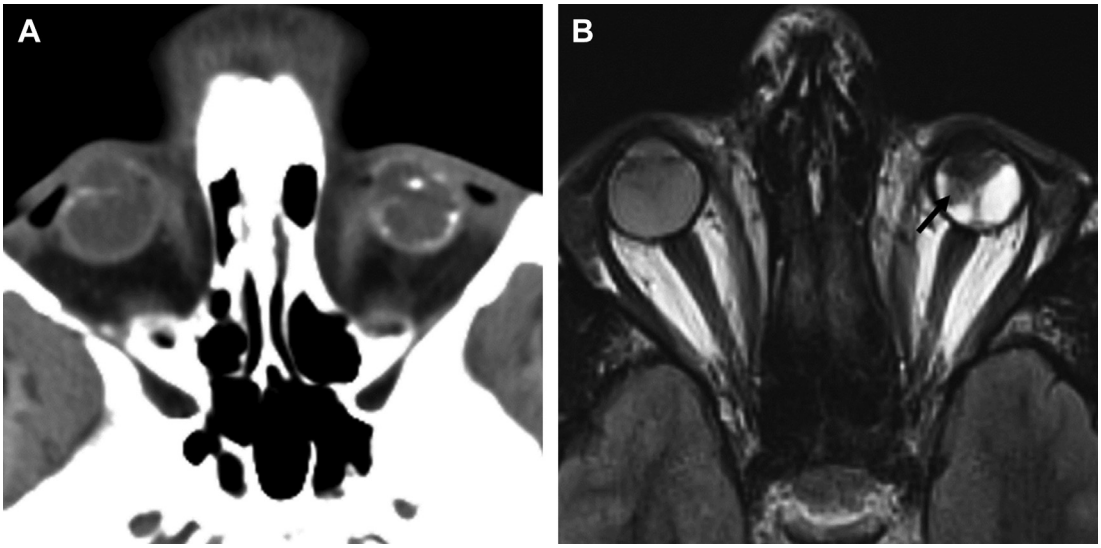

Fig. 14. Retinopathy of prematurity. A 20-year-old ex 24-week premature infant resulting in blindness. (*A*) Axial CT image reveals microphthalmia with foci of mineralization. (*B*) Axial fluid attenuated inversion recovery (FLAIR) MR image shows that there are bilateral retinal detachments with increased signal intensity compared with normal vitreous. There is a small hypointense retrolental lesion on the left (*arrow*).

hemorrhages. In addition, a hypointense retrolental mass may be noted within the globe (see **Fig. 14**B).

Orbital and Ocular Abnormalities with Central Nervous System Malformations

Orbital and ocular anomalies are a feature of several craniofacial disorders as alluded to in earlier sections. Orbital manifestations of NF-1 include spheno-orbital dysplasia, buphthalmos, optic nerve glioma, nerve sheath tumors (neurofibromas, plexiform neurofibromas, and malignant peripheral nerve sheath tumor) (see **Fig. 6**), and occasionally rhabdomyosarcoma (RMS). Orbital lesions in Sturge-Weber syndrome include buphthalmos, glaucoma, venous dysplasia, and venous hypertension (**Fig. 15**A).[25] Tuberous sclerosis is characterized by retinal neuroglial hamartoma (see **Fig. 15**B),[26] and retinal hemangioblastomas are a feature of von Hippel-Lindau disease.[27–30] Joubert syndrome is characterized by abnormal eye movements and optic nerve and/or chorioretinal coloboma, less commonly retinal abnormalities.[31] Several ocular abnormalities occur in congenital muscular dystrophies such as Walker-Warburg syndrome, including cataracts, microphthalmos, buphthalmos, retinal pigmentary changes, PHPV, retinal detachment, vitreous hemorrhage, coloboma, Peter anomaly, and ONH.[32]

Aicardi syndrome is a rare X-linked disorder characterized by agenesis of the corpus callosum, cortical malformations, and chorioretinal lacunae.[33] Additional central nervous system (CNS) and ocular findings are seen with varying frequency, including microphthalmos, anomalous retinal vessels, retinal detachment, dysplasia or coloboma of the optic nerve, persistent pupillary membrane, iris synechiae, posterior iris or choroidal staphylomas, and cataracts.[33,34] Morning glory disc–like anomalies, involving ring-shaped pigment deposits surrounding or within a colobomatous optic nerve head, have also been described in patients with Aicardi syndrome.[33,35]

Nasolacrimal Duct Cyst and Mucocele

Nasolacrimal duct (NLD) cyst and mucocele is typically congenital in nature due to failure of canalization of the distal NLD at the valve of Hasner. This common anomaly is detected incidentally or because of a cystic medial canthal swelling or neonatal nasal obstruction and respiratory distress. On imaging, there is cystic expansion of the intranasal NLD, which protrudes beneath the inferior turbinate, sometimes with enlargement of the lacrimal sac (**Fig. 16**). The differential diagnosis includes meningocele and neuroglial heterotopia, which can appear cystic but project into the nasal cavity above the inferior turbinate.

Lacrimal Gland Anomalies

Aplasia or hypoplasia of the lacrimal gland is a rare disorder that is sometimes associated with aplasia of the salivary glands in the aplasia of the lacrimal and salivary gland syndrome[36] or with abnormalities of the ears, teeth, and digits in the lacrimoauriculodentodigital syndrome.[37] Patients

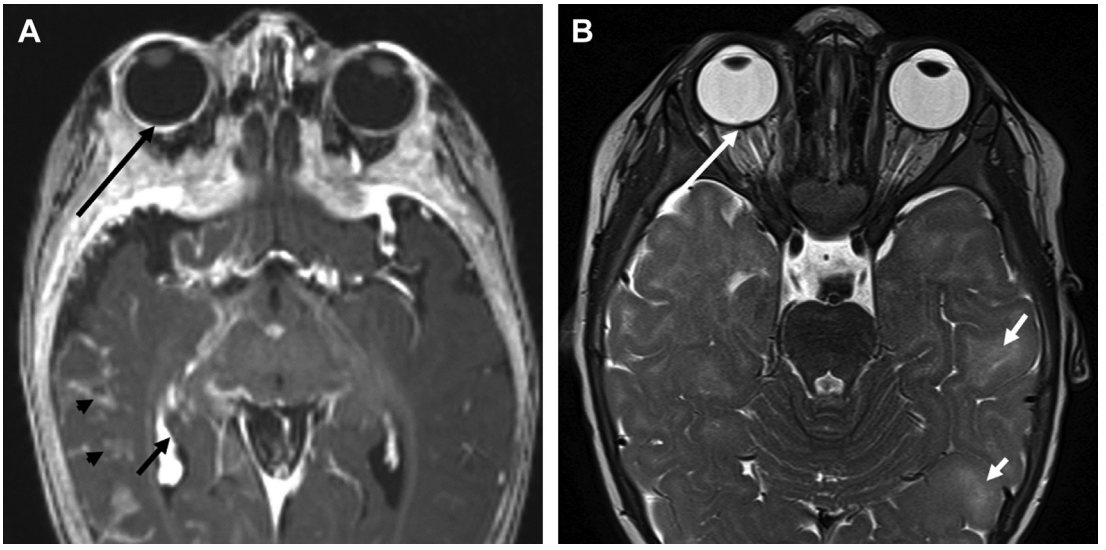

Fig. 15. Ocular abnormalities with CNS malformations. (*A*) Sturge-Weber syndrome (SWS) in a 3-year-old boy. Axial contrast-enhanced T1 magnetization-prepared rapid acquisition gradient-echo (MPRAGE) image shows abnormal right choroidal enhancement (*long arrow*) associated with venous dysplasia. Other typical features of SWS are demonstrated, including enlargement of the right choroid plexus (*short arrow*) and abnormal enhancement around the right temporal lobe related to abnormal venous drainage (*arrowheads*). (*B*) Tuberous sclerosis in a 10-month-old girl. Axial T2-weighted MR image reveals a small retinal neuroglial hamartoma (*long arrow*). Subcortical tubers are seen within the temporal lobes (*short arrows*).

present with alacrima, and imaging reveals absence or marked paucity of lacrimal tissue.

Congenital Cranial Dysinnervation Disorders

The congenital cranial dysinnervation disorders (CCDDs) result from abnormal development of cranial motor nuclei, absence or hypoplasia of affected cranial nerves, and resultant fibrosis of abnormally innervated extraocular muscles. CCDDs include congenital fibrosis of the extraocular muscles (CFEOM; *TUBB3* and other mutations), Bosley-Salih-Alorainy syndrome and Athabascan brain dysgenesis syndrome (*HOXA1*

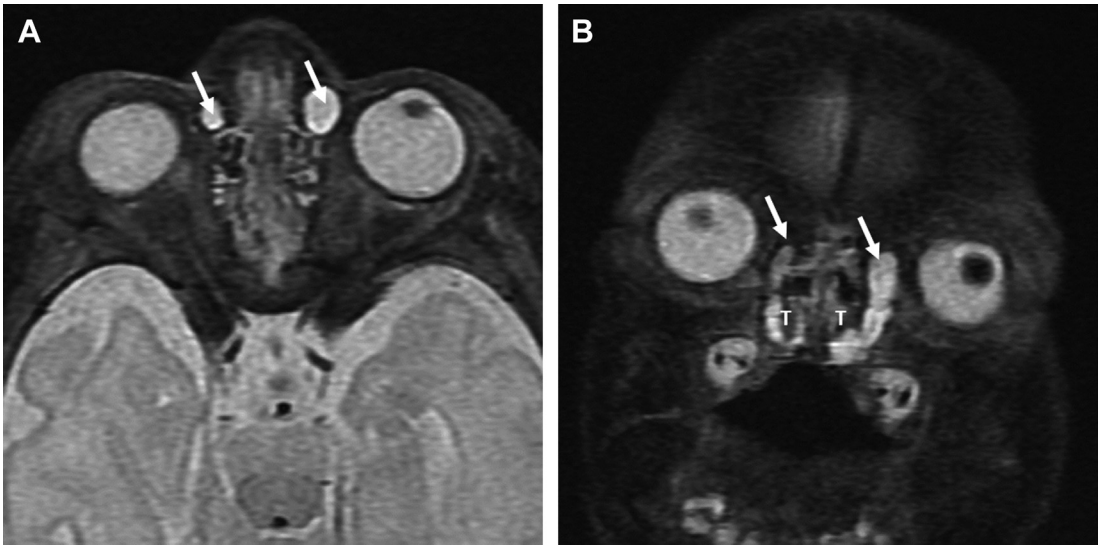

Fig. 16. Nasolacrimal duct cyst (NLDC). A 1-day-old baby girl presenting with nasal obstruction. (*A*) Axial and (*B*) coronal fast spin echo inversion recovery T2-weighted MR images reveal bilateral NLDCs, left larger than right (*arrows*). The coronal image shows that the NLDCs protrude inferior to the inferior turbinates (T). This finding is a helpful distinction from a cephalocele or neuroglial heterotopia that would reside superior to the inferior turbinate.

mutations), *HOXB1* mutations, Duane syndrome (*CHN1, SALL4* and *SALL1* mutations), Moebius syndrome, and horizontal gaze palsy with progressive scoliosis (HGPPS; *ROBO3* mutations).[38] Clinical signs depend on the underlying genetic mutation and affected cranial nerves and include strasbismus, gaze limitation or ophthalmoplegia, ptosis, and poorly reactive pupils. Imaging reveals absence or hypoplasia of the affected cranial nerves and diminutive affected extraocular muscles (**Fig. 17**). Additional malformations of the brain or inner ears occur depending on the underlying genetic mutation.

ORBITAL MASSES

Dermoid and Epidermoid

Dermoids, also known as developmental choristomas, are the most common congenital orbital masses.[13,14] These lesions likely arise from sequestered epithelial rests entrapped in orbital bony sutures and can be subcutaneous or intraorbital in location.[13,39] Both dermoids and the less common epidermoids are composed of cysts lined by keratinized, stratified squamous epithelium with dermoids also containing adnexal structures such as hair and sebaceous glands. Clinically, these lesions manifest as subcutaneous nodules adjacent to the orbital rim or as unilateral proptosis.

Imaging does not reliably distinguish between dermoids and epidermoids. On contrast-enhanced CT, these lesions present as well-defined low-density masses that remodel adjacent bone, with mild thin rim contrast enhancement. Thick, irregular rim of enhancement suggests inflammation secondary to rupture. Fatty components usually present as negative attenuation values within the mass and a fat-fluid level may occasionally be noted within a dermoid. Calcification is seldom seen in children. On MR imaging, dermoids/epidermoids typically demonstrate hypointensity on T1-weighted and variable, usually hyperintense signal on T2-weighted images with decreased diffusivity. Fat contents result in T1 shortening (**Fig. 18**). There is minimal, if any, thin peripheral contrast enhancement.

VASCULAR LESIONS

The most common vascular lesions in infants and children are infantile hemangiomas (IHs), lymphatic malformations (LMs), and venous malformations (VMs). MR imaging is the modality of choice for characterizing and distinguishing between these lesions based on degree of vascularity, the presence of a solid or cystic mass, fluid-fluid levels/hemorrhage or phleboliths, and the degree of contrast enhancement.

Lymphatic Malformation

LM is an unencapsulated mass of thin-walled lymphatic channels and represents the most common vascular malformation in childhood.[40–42] Clinically, LMs grow commensurate with growth of the

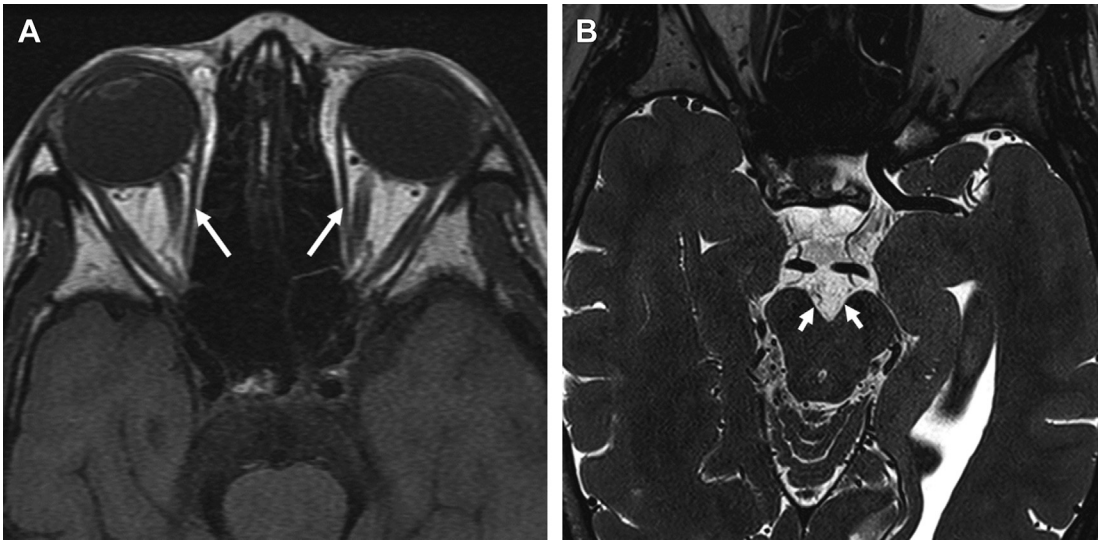

Fig. 17. Congenital cranial dysinnervation disorder. Teenaged boy with Moebius-type syndrome and TUBB 3 mutation. Clinical examination revealed facial palsy and limited adduction and elevation of the eyes. (*A*) Axial T1-weighted MR image shows diminutive medial rectus muscles bilaterally (*arrows*). The superior and inferior rectus muscles were also small (not shown). (*B*) Axial 3D T2 SPACE image at the level of the midbrain and interpeduncular cistern demonstrates absence of cranial nerve III bilaterally (*arrows*).

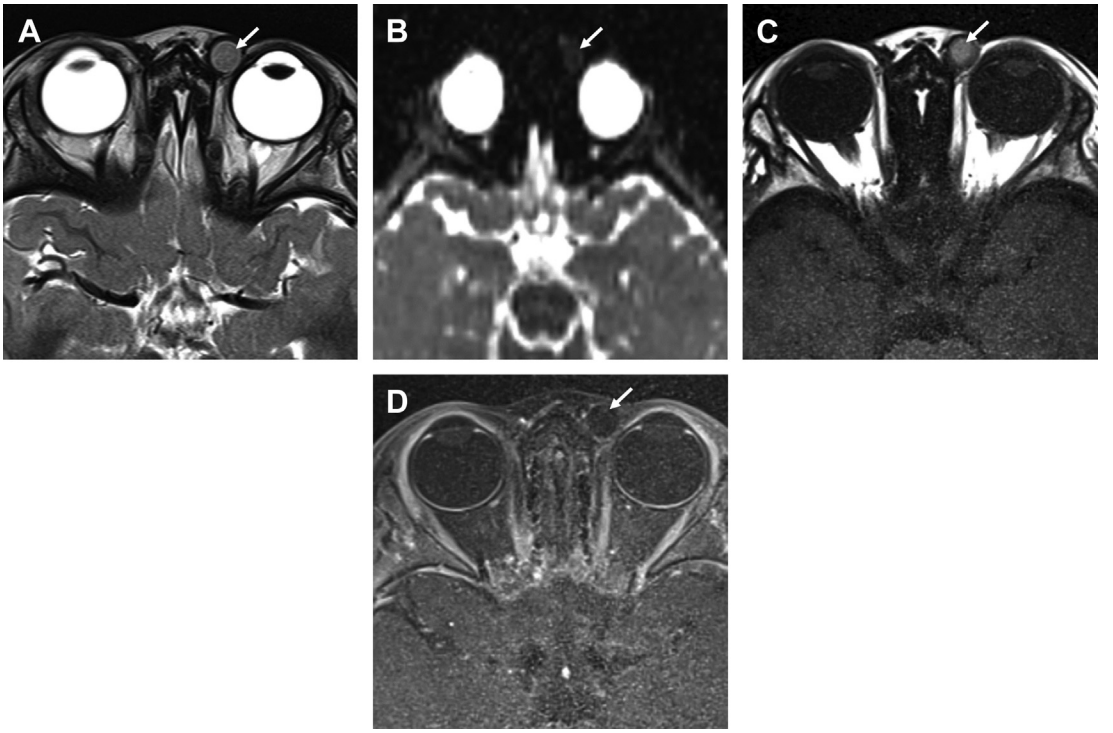

Fig. 18. Dermoid cyst. A 2-year-old boy with a left medial canthal mass. (*A*) Axial T2-weighted (T2W) MR image shows a sharply circumscribed left preseptal mass (*arrow*) that is isointense with gray matter. (*B*) Diffusion-weighted imaging apparent diffusion coefficient map reveals that the lesion has decreased diffusivity (*arrow*). (*C*) Axial T1-weighted (T1W) image demonstrates mild T1 shortening within the mass (*arrow*). (*D*) Gadolinium-enhanced fat-suppressed T1W image shows that the lesion does not enhance (*arrow*). These features are consistent with a dermoid cyst, which was confirmed following surgical excision. Dermoids have variable, typically homogeneous signal intensity on T1W and T2W images and typically show decreased diffusivity and minimal, if any, marginal enhancement.

patient but may enlarge suddenly as a result of the propensity to bleed or become infected.

On US, CT, and MR imaging, LMs appear microcystic or macrocystic, lobulated, and septated. Transpatial involvement of the intraconal and extraconal spaces may occur. Characteristic fluid-fluid levels usually associated with hemorrhage are well seen on MR imaging and are a typical feature of LM (Fig. 19). Hemorrhage also alters the signal intensity on MR imaging, sometimes

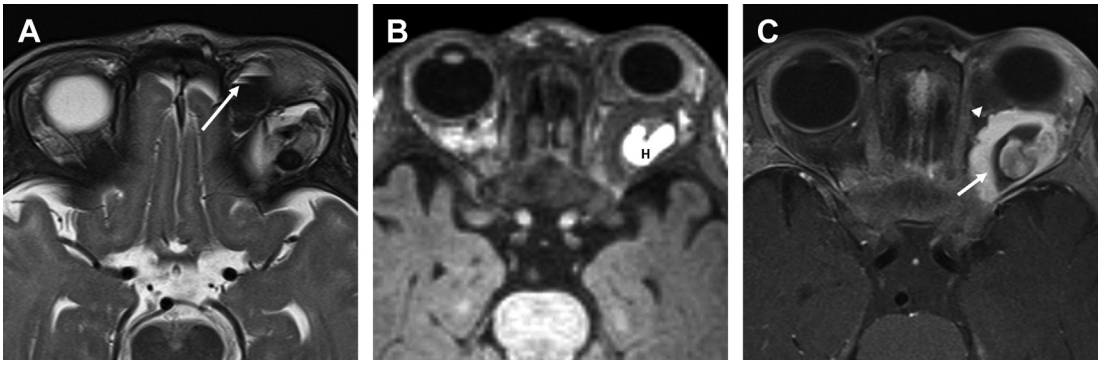

Fig. 19. Lymphatic malformation (LM) with venous component. An 8-month-old girl with recent-onset left proptosis. (*A*) Axial T2-weighted MR image reveals a macrocystic, hemorrhagic left intraconal mass that contains fluid-fluid levels (*arrow*), characteristic of LM complicated by hemorrhage. (*B*) Axial T1-weighted (T1W) MR image shows the hyperintense hemorrhage (H). (*C*) Gadolinium-enhanced fat-suppressed T1W MR image shows some enhancement of the lesion consistent with a venous component (*arrow*). Nonenhancing LM is also seen (*arrowhead*).

producing T1 and T2 shortening. Pure LMs demonstrate mild enhancement of septations only, and the contained fluid does not enhance. High flow vascularity is not a feature of LMs. Enhancement of fluid within the cystic septations is consistent with a venous component (see Fig. 19), as evidenced also by the presence of phleboliths. Evaluation of the brain is indicated to assess for associated intracranial venous lesions such as cavernous malformations, prominent developmental venous anomalies, and occasionally high-flow arteriovenous fistulae.[42]

Surgery to reduce compression on the optic nerve and improve cosmetic appearance may be associated with recurrence. Sclerotherapy with sodium tetradecyl sulfate or OK-432 may be helpful in the management of macrocystic LMs; however, the use of sclerotherapy in the postseptal orbit is limited because of the risk of postprocedural increased intraorbital pressure caused by swelling.[43]

Venous Malformation

Orbital VM is a distensible low-flow lesion characterized by dilated venous channels. VMs increase in size with Valsalva maneuver, crying, and straining. VMs must be distinguished from orbital varices that arise secondary to arteriovenous shunting or venous occlusive diseases such as venous sinus thrombosis.[44]

US, CT, and MR imaging show a well-defined cystic, septated lesion. The venous blood enhances gradually with contrast. VMs are sometimes complicated by thrombosis, which affects the echogenicity on US and density or signal intensity on CT and MR imaging, respectively. Phleboliths are a characteristic feature of VMs (Fig. 20). As with LMs, high-flow vascularity is not a feature of VMs. As mentioned, sometimes lesions demonstrate mixed characteristics of VM and LM with associated intracranial VMs.[41]

Arteriovenous Malformation and Carotid Cavernous Fistula

Orbital AVMs are uncommon high-flow vascular anomalies that may present with proptosis and orbital bruit. Imaging usually consists of MR imaging with MRA and CTA or conventional angiography to demonstrate the arterial and venous anatomy and the presence of a nidus or tangle of vessels between the enlarged arterial feeders and early draining veins. Therapeutic options vary depending on the anatomy of the lesion and can include endovascular embolization and/or surgery.

A carotid cavernous fistula (CCF) is an abnormal connection between the internal carotid arterial system and the cavernous venous sinuses. Direct CCF can be caused by craniofacial injury or trauma. Spontaneous CCF may develop from rupture of an intracavernous aneurysm or secondary to vessel weakness in conditions such as Ehlers-Danlos syndrome or fibromuscular dysplasia.[45–48] Although CCF is uncommon in children, the signs and symptoms seem to be similar to those seen in adults.[45–47]

CT and MR imaging demonstrate dilation of the superior ophthalmic vein and exophthalmos with enlarged extraocular muscles (Fig. 21A). On MR images, there may be distension of the cavernous sinuses with abnormal cavernous sinus flow voids. Conventional angiography identifies the exact location of the CCF so as to plan definitive treatment (see Fig. 21B).

NEOPLASMS

Pediatric ophthalmic tumors are classified into orbital neoplasms and intraocular tumors. Many

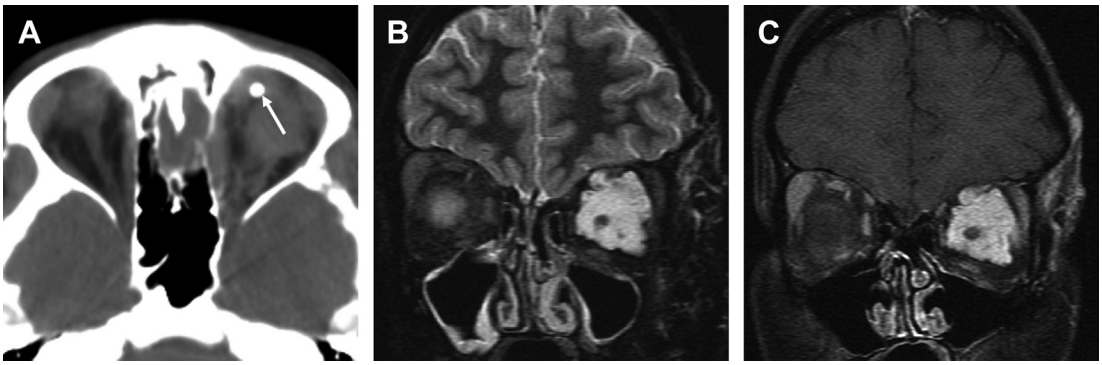

Fig. 20. Venous malformation (VM). Teenaged girl with blue rubber bleb nevus syndrome. (*A*) Axial CT image shows a phlebolith within the left orbit (*arrow*). (*B*) Coronal T2 short tau inversion recovery (STIR) MR image shows a large, hyperintense, multicystic intraconal lesion. (*C*) Coronal fat-suppressed contrast-enhanced T1-weighted MR image shows that the lesion enhances. These features are diagnostic of VM.

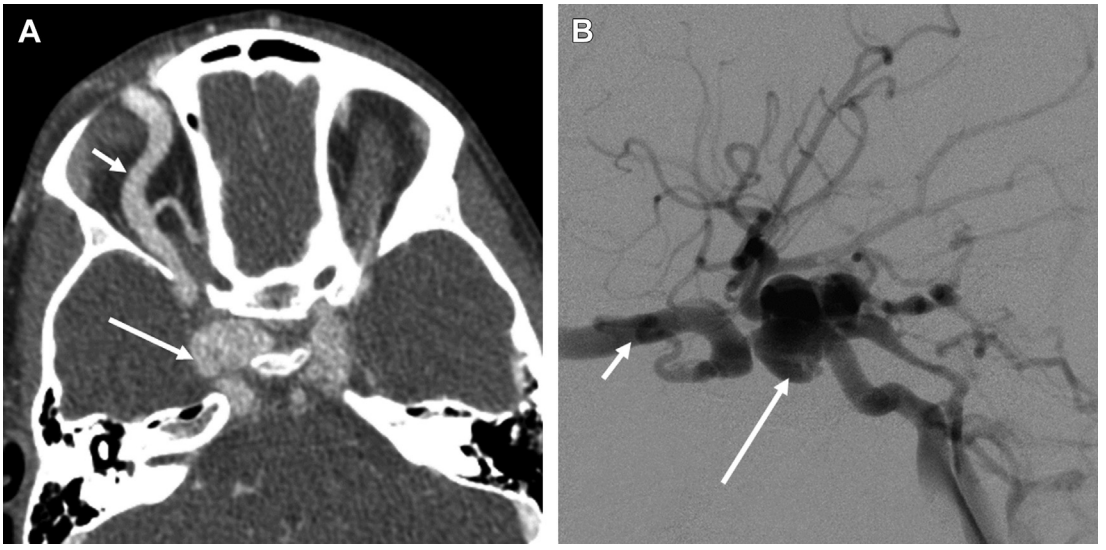

Fig. 21. Carotid cavernous fistula (CCF). A 6-year-old girl with remote eye trauma, headaches, and vertigo. (*A*) Axial contrast-enhanced CT shows marked enlargement of the right superior ophthalmic vein (SOV) (*short arrow*) and the right cavernous sinus/cavernous right internal carotid artery (ICA) (*long arrow*). (*B*) Cerebral angiography with selective right ICA injection confirms the direct CCF (*long arrow*) with principal drainage into an enlarged right SOV (*short arrow*) and both cavernous sinuses and their tributaries (*long arrow*).

of these tumors are benign; however, they have a significant impact on vision and may result in significant morbidity and mortality. This section presents common orbital and intraocular lesions.

Orbital Neoplasms

Infantile hemangioma

IH is the most common vascular tumor of infancy. Orbital hemangioma typically presents shortly after birth with proptosis and/or a strawberry red mass involving the periorbital skin. IH is characterized by proliferation with rapid growth during the first year of life followed by gradual involution by 7 to 8 years of age.[40,49] True congenital hemangiomas are uncommon and are divided into those that involute rapidly (rapidly involuting congenital hemangioma) and those that do not (noninvoluting congenital hemangioma). Imaging is indicated to detect the extent of the lesion and to distinguish IH as a cause of proptosis from other orbital masses.

The imaging features of IH are characteristic and diagnostic. US demonstrates a hyperechoic, bosselated mass with prominent high-flow vascularity noted on color Doppler US. CT demonstrates a well-defined mass with intense homogeneous enhancement. MR imaging demonstrates a solid, circumscribed, and somewhat lobulated mass that is isointense with white matter on T2-weighted images. Characteristic signal voids are a feature of proliferating IH and reflect prominent vascularity. Proliferating IH also demonstrates intense, homogeneous contrast enhancement (**Fig. 22**). Involution is associated with decreased vascularity and enhancement and increasing fibrofatty matrix. Bony remodeling may occur. IH must be distinguished from cystic lesions such as LMs, VMs, or mixed low-flow vascular anomalies and from solid tumors such as RMS. The key feature distinguishing IH from RMS is the intense enhancement and vascularity of IH. Orbital hemangioma can be associated with other anomalies as a manifestation of PHACES association.[21]

Most hemangiomas are treated conservatively anticipating involution. However, tumors that compromise vision can be treated with systemic propranolol.

Teratoma

Orbital teratomas are derived from more than 1 primitive germ cell layer and are usually benign. CT and MR imaging demonstrate a multilocular cystic and solid mass (comprising fat, calcification, or both) within the orbit that may displace the normal globe and result in expansion of the bony orbit. Surgical resection of benign teratoma is curative.

Rhabdomyosarcoma

RMS is the most common mesenchymal tumor in children[50–52] and the most prevalent pediatric extraocular orbital malignancy.[53,54] Two histologic subtypes of RMS are prevalent in children: the embryonal subtype is the most common orbital

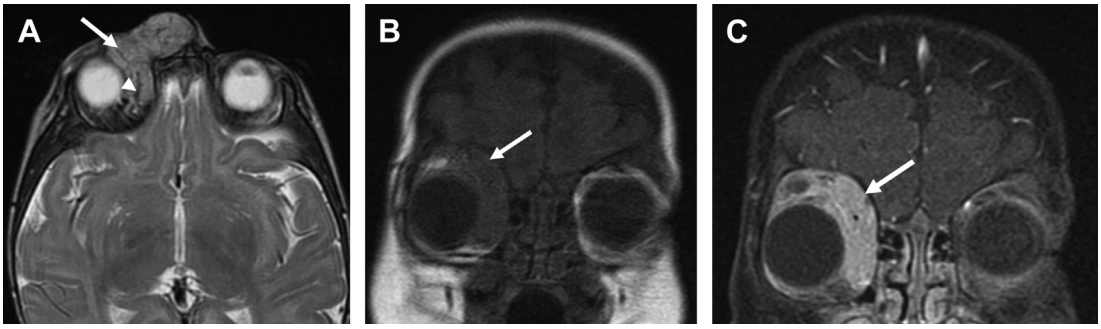

Fig. 22. Infantile hemangioma. A 4-month-old girl with ptosis. (*A*) Axial T2-weighted MR image shows a sharply marginated extraconal, preseptal, and frontonasal mass (*arrow*) that is isointense with white matter and contains vascular signal voids (*arrowhead*). (*B*) Coronal T1 precontrast and (*C*) postcontrast fat-suppressed T1-weighted images demonstrate the avidly enhancing soft-tissue mass (*arrow*) centered within the medial aspect of the right orbit. These findings are characteristic of proliferating infantile hemangioma.

variant and is the least aggressive subtype; the more aggressive alveolar subtype is less prevalent in the orbit.[55] Orbital RMS typically presents with rapidly progressive, unilateral proptosis and diplopia. The median age of presentation is 6 to 8 years,[56] although the alveolar subtype generally affects older children or adolescents.[43]

CT, PET-CT, and MR imaging are important in the preoperative evaluation and staging of orbital RMS and provide complementary information. CT demonstrates osseous erosion and/or remodeling, whereas MR imaging demonstrates soft-tissue characterization and intracranial extension. MR imaging and PET-CT are used for follow-up and assessment of therapeutic response.

On CT images, orbital RMS generally appears as an extraconal, ovoid, well-circumscribed mass that is isodense relative to muscle, with moderate to marked contrast enhancement. Remodeling of bone or frank aggressive bony destruction can occur. Eyelid thickening is a common associated finding whether or not the tumor extends to the eyelid.

On MR imaging, RMS is isointense to muscle on T1-weighted images and hyperintense to muscle on T2-weighted images, often appearing isointense with cerebral cortex, with decreased diffusivity and moderate to marked contrast enhancement (**Fig. 23**). The mass may distort or displace but does not typically invade the globe. The extraocular muscles are similarly distorted and are sometimes inseparable from tumor. Invasion of adjacent paranasal sinuses or intracranial contents may be seen, and comparison of nonenhanced and enhanced T1-weighted images helps distinguish tumor extension into the paranasal sinuses from trapped sinus secretions.

Many benign and malignant entities share clinical features of RMS. Proliferating IH presents in younger children and demonstrates characteristic vascular flow voids and more intense and homogeneous enhancement. RMS may appear indistinguishable from orbital lymphoma, which is the chief differential diagnostic consideration.

Orbital RMS treatment usually consists of surgical resection, followed by radiation therapy and chemotherapy. Prognosis depends on histologic and molecular subtype and feasibility of complete surgical resection. Parameningeal spread of tumor suggests a worse prognosis. The 5-year survival rates for embryonal and alveolar subtypes are 94% and 74%, respectively.[51]

Langerhans cell histiocytosis

Langerhans cell histiocytosis (LCH) represents a spectrum of disease ranging from benign unifocal bone disease to more aggressive multisystem disease.[57] Eosinophilic granuloma, the most localized and benign form of LCH often presents as unifocal bone disease with orbital bone involvement; the lesion usually manifests in children (boys > girls) younger than 4 years with proptosis, ptosis, erythema, and enlarging palpebral fissures.[53]

CT and MR imaging help delineate the extent of disease and bony involvement. On CT, LCH typically appears as a well-defined, moderately to markedly enhancing osteolytic soft-tissue mass. Bony margins are characteristically sharply defined with beveled edges (**Fig. 24**A).

On MR images, the soft-tissue component can be heterogeneous or homogeneous on T1-weighted images and hyperintense, isointense, or hypointense relative to cerebral cortex on T2-weighted images. Moderate to marked homogeneous or heterogeneous enhancement occurs. MR imaging is the modality of choice for demonstrating intracranial extension. The MR features of LCH can simulate more aggressive sarcomatous lesions or metastasis; however, the CT features of LCH are usually characteristic (see

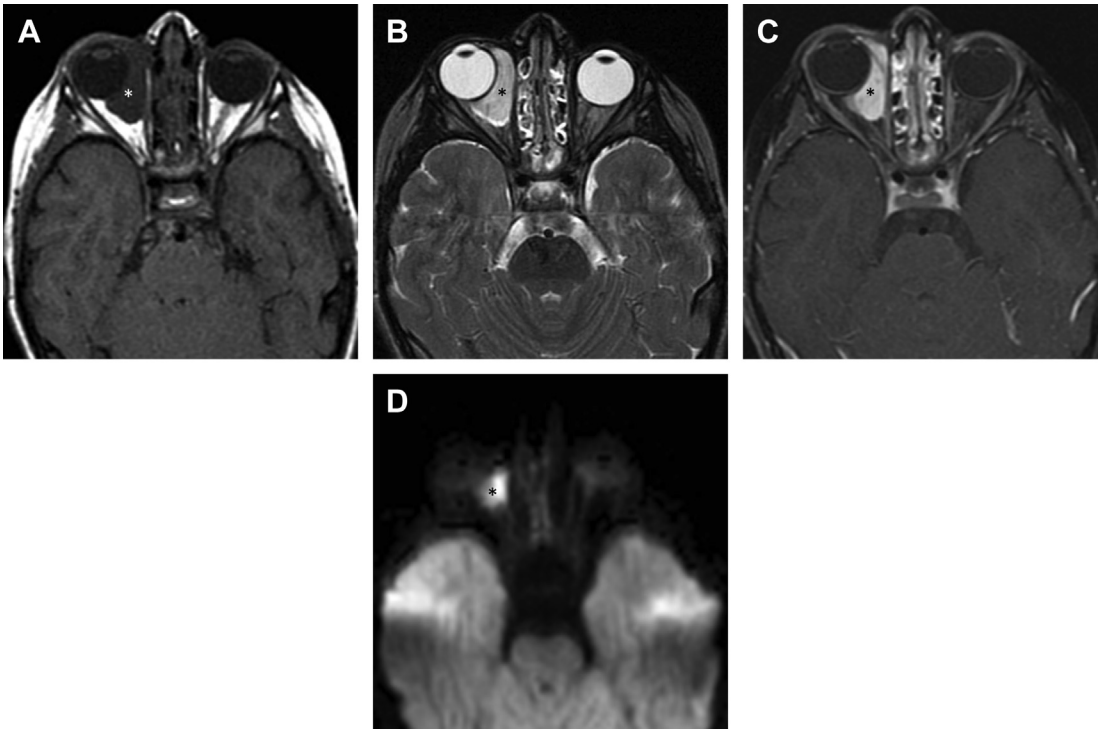

Fig. 23. Embryonal rhabdomyosarcoma. A 4-year-old boy with right proptosis. (*A*) Axial T1-weighted (T1W) MR image shows a mass (*asterisk*) along the medial aspect of the orbit, which is isointense to muscle. (*B*) Axial T2-weighted MR image shows that the mass is hyperintense to muscle. (*C*) Axial fat-suppressed contrast-enhanced T1W image demonstrates moderate tumoral enhancement. (*D*) Diffusion-weighted imaging shows that there is decreased diffusivity within portions of the mass (*asterisk*). The lack of vascular flow voids distinguishes rhabdomyosarcoma from hemangioma.

Fig. 24). In young children, the differential diagnosis includes other histiocytic tumors such as juvenile xanthogranuloma. Surgical resection of isolated lesions is usually curative.

Leukemia

Chloroma (granulocytic sarcoma) represents the most common form of acute myelogenous leukemic involvement of the orbit.[13,58] These solid tumors typically present in children with proptosis and diplopia. These lesions may be bilateral in contrast to RMS.[13]

On CT, chloroma presents as an irregular mass of homogeneous density with poor contrast enhancement and frequent lytic, permeative bony erosion. On MR imaging, the lesion is isointense to muscle on T1- and T2-weighted images with decreased diffusivity and variable, homogeneous enhancement (Fig. 25). In addition to chloromas, orbital leukemia may result in optic nerve infiltration; intraocular involvement of the choroid, retina, or anterior chamber; and infiltration of extraocular muscles. The differential diagnosis includes RMS, lymphoma, and metastatic neuroblastoma.

Treatment of chloroma is usually systemic chemotherapy and bone marrow transplantation.[13] Leukemic infiltration of the optic nerve is a medical emergency because of the potential for permanent visual loss if left untreated. The treatment in such cases is low-dose radiation therapy often combined with intrathecal chemotherapy.[13]

Lymphoma

Lymphoproliferative disease accounts for approximately 10% of pediatric orbital tumors; lymphoid hyperplasia accounts for 10% to 40% of the lesions, whereas non-Hodgkin lymphoma accounts for 60% to 90% of the lesions.[59] Patients typically present with gradual, painless progressive proptosis.

On CT and MR imaging, lymphoma typically presents as a mass resulting in associated enlargement of the lacrimal glands or extraocular muscles. Lymphoma is characteristically homogeneous on T2-weighted MR images and appears isointense with white matter, with mild homogeneous contrast enhancement (Fig. 26). The differential diagnosis for a defined mass involving the extraocular muscles is primarily RMS. However,

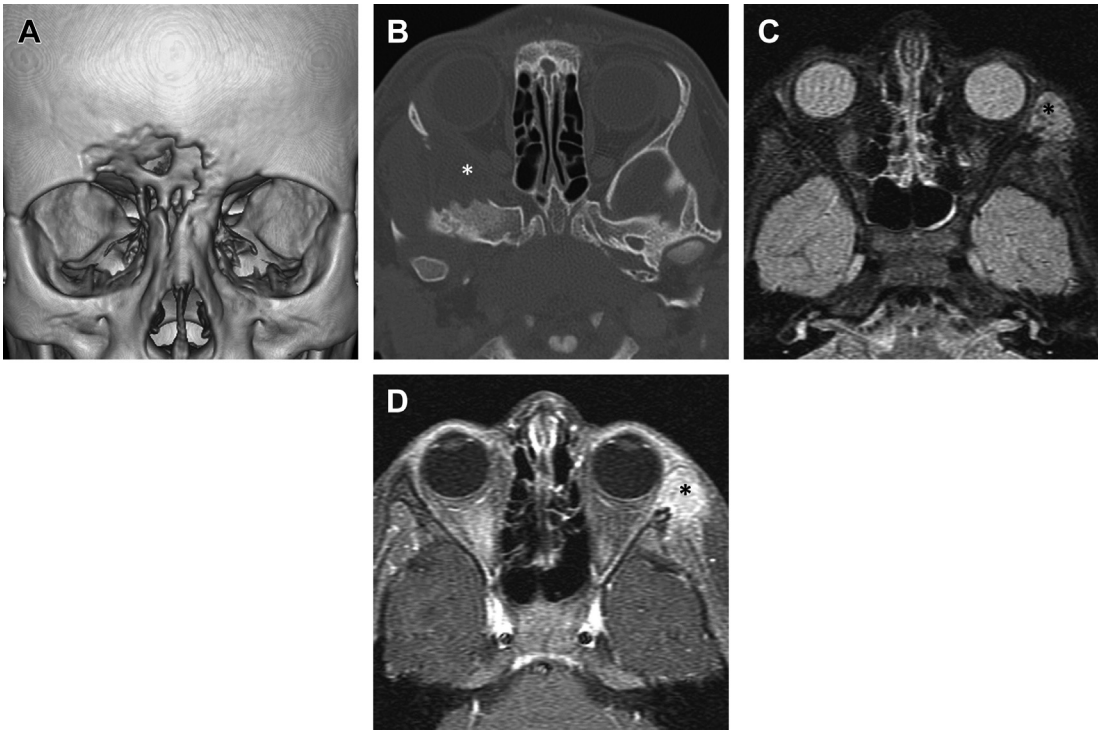

Fig. 24. Langerhans cell histiocytosis (LCH). (*A*) Three-dimensional CT in a 5-year-old boy with supraorbital LCH shows sharply marginated bony destruction with beveled edges. (*B*) Axial bone window CT in a 2-year-old boy with LCH showing sharply marginated bony destruction of the lateral wall of right sphenoid bone (*asterisk*). (*C*) Axial T2 STIR MR in a 4-year-old male with LCH shows a slightly heterogeneous mass that is isointense with cortex eroding the lateral wall of the left orbit (*asterisk*). (*D*) Contrast-enhanced axial T1-weighted MR in the same child shows that the mass enhances avidly (*asterisk*).

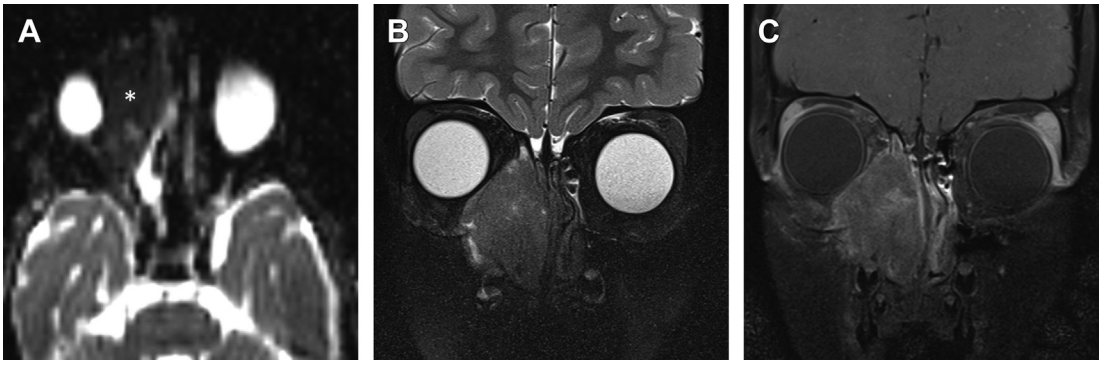

Fig. 25. Leukemia. A 3-year-old girl with prior history of acute myelogenous leukemia (AML) with recent right nasal drainage and proptosis. (*A*) Axial diffusion-weighted imaging apparent diffusion coefficient map shows a right sinonasal mass characterized by decreased diffusivity (*asterisk*). (*B*) Coronal fat-suppressed T2-weighted (T2W) MR image reveals the homogeneous, hypointense tumor that is isointense with white matter. The sinonasal tumor erodes the medial and inferior walls of the right orbit. (*C*) Coronal contrast-enhanced fat-suppressed T1-weighted image shows mild enhancement of the tumor. Chloroma was confirmed after biopsy. The homogeneous hypointensity on T2W image is indistinguishable from lymphoma.

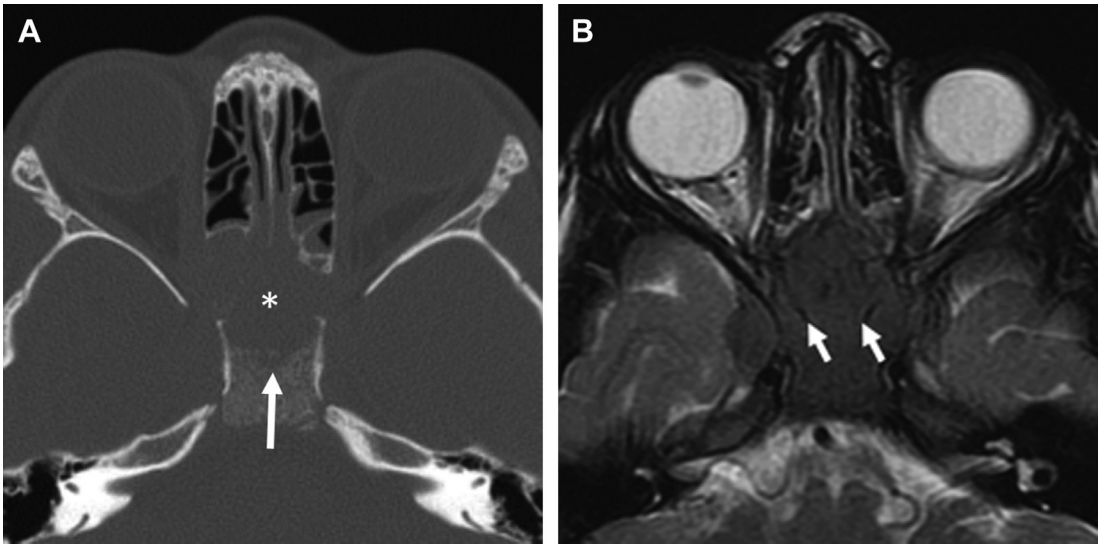

Fig. 26. Lymphoma. A 4-year-old boy with headache and vomiting. (*A*) Axial CT bone window reveals an erosive sphenoethmoidal mass (*asterisk*) extending to the orbital apices. There is a permeative pattern of bony destruction in the sphenoid bone (*arrow*), consistent with an aggressive process. (*B*) Axial T2-weighted MR shows the homogeneous and markedly hypointense tumor invading the cavernous sinuses and surrounding and compressing the optic nerves (*arrows*). Biopsy revealed Burkitt lymphoma.

the differential diagnosis for lymphoma involving the bony orbit also includes leukemia, other sarcoma, and metastasis.

Malignant lymphoproliferative lesions confined to the orbit are usually treated with radiation depending on histologic type.

Neuroblastoma metastases

Neuroblastoma is the most common primary childhood cancer to metastasize to the orbits.[60,61] The most common clinical presentation of orbital neuroblastoma metastases is unilateral or bilateral proptosis and periorbital or eyelid ecchymosis (raccoon eyes) in a child younger than 2 years.[53]

On CT, metastases appear as ill-defined, hyperdense, sometimes mineralized masses. There is permeative, lytic destruction of bone (**Fig. 27**A), sometimes with a characteristic spiculated periosteal reaction. On MR imaging, the lesions appear isointense with cerebral cortex on T2-weighted images, with decreased diffusivity and heterogeneous or homogeneous contrast enhancement (see **Fig. 27**B).

Treatment of metastatic neuroblastoma depends on clinical features, histopathologic analyses, chromosomal abnormalities, and expression of the N-Myc oncogene.[53]

Intraocular Neoplasms

Retinoblastoma

Retinoblastoma is the most common intraocular malignancy of childhood, usually manifesting before 5 years of age. Retinoblastomas are bilateral in 40% of cases.[62] Trilateral retinoblastoma (bilateral ocular tumors and a midline intracranial neuroblastic tumor, typically pineal) and quadrilateral retinoblastoma (bilateral ocular disease, pineal and suprasellar tumors) may be present.[62] There are both heritable and nonheritable forms of retinoblastoma.[62] In the heritable form, the first mutation is constitutional, whereas the second is somatic, which causes early onset of bilateral or multifocal tumors in most patients.[63] These children are at increased risk for the development of other head and neck malignant tumors (eg, osteogenic sarcoma and RMS). In the nonheritable form, both allelic mutations are somatic, resulting in unilateral tumors with an older age of presentation than the heritable form.[63]

Leukocoria, in which the normal red reflex of the retina is replaced by yellowish-white light reflecting off the tumor, occurs in 56% to 72% of patients with retinoblastoma and is the most common initial presenting sign. Other less common clinical manifestations include decreased vision, anisocoria, spontaneous hyphema, and heterochromia iridis.[62]

Imaging plays an important role in confirming the diagnosis of retinoblastoma and determining staging. CT demonstrates a hyperattenuating and typically calcified mass in the posterior globe (**Fig. 28**A). The mass may extend into the vitreous or subretinal space, sometimes resulting in retinal detachment. The size of the globe is normal or slightly enlarged.

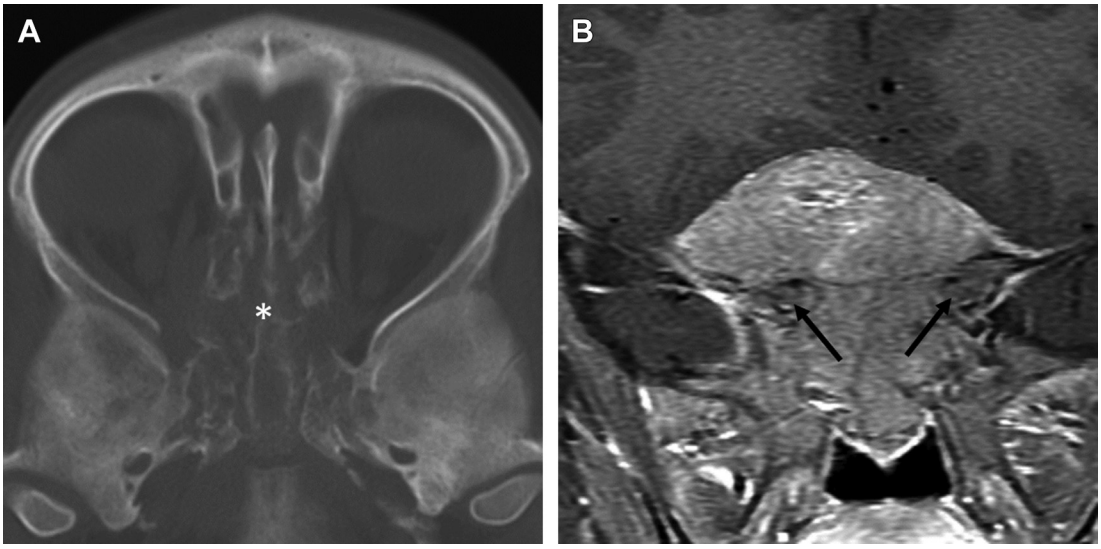

Fig. 27. Neuroblastoma. A 3-year-old boy with a headache. (*A*) Axial CT image showing lytic, permeative destruction of the sphenoid and ethmoid bones (*asterisk*). (*B*) Coronal contrast-enhanced fat-suppressed T1-weighted MR image shows a large, expansile, enhancing sphenoid bone mass encircling the optic nerves (*arrows*). Although the appearance on MR imaging could simulate a meningioma in an older child, the appearance is highly characteristic of neuroblastoma in a child of this age. The tumor demonstrated metaiodobenzylguanidine (MIBG) avidity (not shown) with a suprarenal primary neuroblastoma.

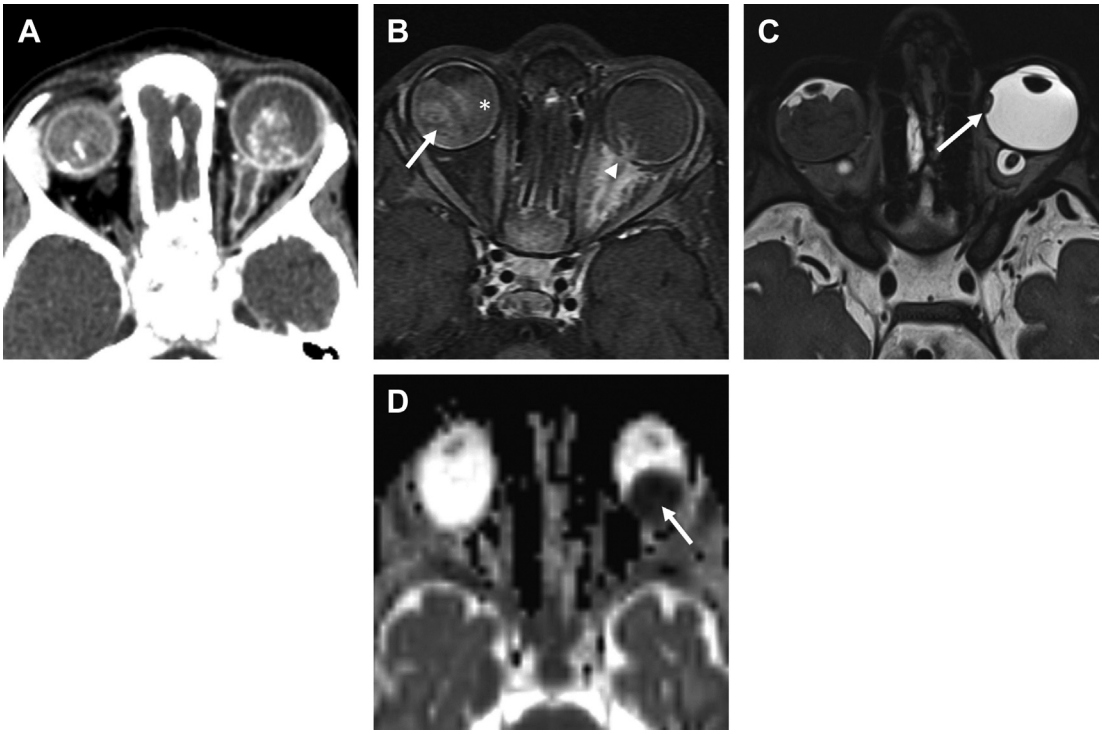

Fig. 28. Retinoblastoma (RB). (*A*) Axial contrast-enhanced CT in a 17-month-old girl with leukocoria. Calcified masses are demonstrated within the globes bilaterally consistent with RB. On the left, there is abnormal density and enhancement due to extension of tumor along the optic nerve. (*B*) Axial contrast-enhanced fat-suppressed T1-weighted MR image shows that the right ocular tumor (*arrow*) is associated with retinal detachment (*asterisk*). There is extensive enhancement around and within (*arrowhead*) the left optic nerve due to invasion by tumor. (*C*) Axial T2 SPACE MR image showing bilateral RB in a 30-month-old boy with the bilateral hypointense RB. The smaller left RB (*arrow*) is well contrasted against the hyperintense vitreous. (*D*) Axial diffusion-weighted imaging apparent diffusion coefficient map showing decreased diffusivity of a left RB (*arrow*) in a 3-month-old boy.

Three-tesla MR imaging is the modality of choice for evaluating patients with suspected or known retinoblastoma and for surveillance for synchronous and metachronous tumors of the CNS and head and neck. Retinoblastoma approximates the signal of gray matter on MR imaging, with the tumor appearing hyperintense to vitreous on T1-weighted images and hypointense to vitreous on T2-weighted images, with decreased diffusivity and contrast enhancement (see **Fig. 28**B–D). A small percentage of retinoblastomas present with a diffuse infiltrative pattern without a discrete mass or calcifications; these can be challenging to diagnose on imaging.[62]

The differential diagnosis includes other causes of leukocoria such as PHPV, Coats disease, toxocara endophthalmitis, and ROP (see **Box 1**). PHPV, Coats disease, and toxocara endophthalmitis typically lack calcifications early in the disease. ROP can be bilateral and may show calcification but is distinguished by a history of prematurity and microphthalmia (see **Fig. 14**).

Treatment of retinoblastoma is complex and is based on the size, location, and extent of tumor. Small tumors are treated with cryoablation, laser photocoagulation, chemotherapy, or plaque radiation therapy.[62] Larger tumors may be treated with chemoreduction followed by surgical resection. Tumors larger than half the globe are treated with enucleation.

Medulloepithelioma

Medulloepithelioma (diktyoma or teratoneuroma) is a rare embryonal neoplasm that arises from the primitive medullary epithelium of the ciliary body. The mean age of presentation of this tumor is 5 years, with the most common presenting symptoms being poor vision and pain.[62]

On CT, medulloepithelioma appears as a dense irregular mass arising from the ciliary body with associated dystrophic calcifications seen in approximately 30% of cases. On MR imaging, the lesion is moderately hyperintense to vitreous on T1-weighted images and hypointense on T2-weighted images with moderate to marked contrast enhancement. Tumor involving the ciliary body should suggest the diagnosis; however, if tumor arises from or spreads to the retina, histopathologic examination may be required to differentiate medulloepithelioma from retinoblastoma.

Treatment is usually enucleation to prevent local recurrence; however, distant metastasis and mortality are uncommon.

Optic pathway glioma

Optic pathway glioma has been covered in another article elsewhere in this issue by Tantiwongkosi and colleagues and is not discussed again in this section.

Papilledema and pseudopapilledema

Papilledema, defined as optic disc swelling, often occurs as a result of raised intracranial pressure

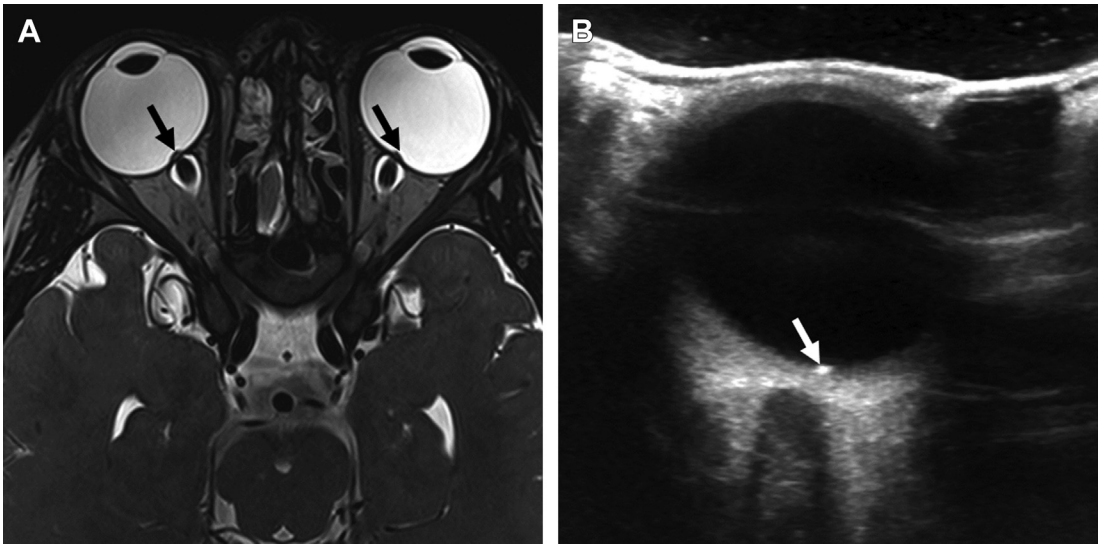

Fig. 29. Papilledema and drusen. (*A*) A 3-year-old boy with exotropia, myopia, and papilledema. (*A*) Axial 3-dimensional T2 SPACE MR image shows elevation of the optic papillae bilaterally (*arrows*). Mildly abnormal contour of the globes may be attributable to myopia with early staphyloma. No intracranial mass, hydrocephalus, or other cause for papilledema was seen. Lumbar puncture confirmed elevated opening pressure consistent with idiopathic intracranial hypertension. (*B*) Ultrasound image in an 18-year-old girl with suspected papilledema reveals an echogenic focus (*arrow*) at the optic papilla consistent with drusen.

from intracranial neoplasms, hemorrhage, idiopathic intracranial hypertension (pseudotumor cerebri), venous sinus thrombosis, or hydrocephalus.[64,65] Papilledema is usually a bilateral condition, although asymmetry may be seen on clinical examination. Imaging is indicated to evaluate the underlying cause. The modality of choice is MR imaging, as it allows visualization of the entire optic pathway, brain, and dural venous sinuses. MR imaging findings suggestive of papilledema include enlargement of the optic nerve sheaths, flattening of the posterior sclera, protrusion of the optic discs into the vitreous humor, and tortuosity of the optic nerves (**Fig. 29**A). Beyond evaluation of the optic pathways, MR imaging and MRV of the brain should be performed, with contrast as indicated, to evaluate for the various causes of papilledema.

Pseudopapilledema like papilledema may present with optic disc swelling but unlike papilledema is not associated with raised intracranial pressure and is typically a normal physiologic variation or secondary to causes such as Down syndrome, high hyperopia, or optic disc drusen.[64] Drusen usually presents with intraocular calcifications; when located at the optic nerve head, bulky drusen may mimic papilledema on fundoscopy and on thin-section, high-resolution T2-weighted MR images. In such patients, ocular US demonstrates the characteristic echogenic, mineralized focus at the optic papilla (see **Fig. 29**B), appearing as punctate increased density at the optic papilla on CT.

SUMMARY

This article discusses a wide spectrum of pediatric orbital diseases commonly encountered in clinical practice. By understanding the clinical presentation and characteristic imaging characteristics of pediatric ophthalmic disease, a narrow differential diagnosis can be formulated and appropriate timely management can be initiated.

REFERENCES

1. Albernaz VS, Castillo M, Hudgins PA, et al. Imaging findings in patients with clinical anophthalmos. AJNR Am J Neuroradiol 1997;18(3):555–61.
2. Verma AS, Fitzpatrick DR. Anophthalmia and microphthalmia. Orphanet J Rare Dis 2007;2:47.
3. Fuhrmann S. Eye morphogenesis and patterning of the optic vesicle. Curr Top Dev Biol 2010;93:61–84.
4. Voronina VA, Kozhemyakina EA, O'Kernick CM, et al. Mutations in the human RAX homeobox gene in a patient with anophthalmia and sclerocornea. Hum Mol Genet 2004;13(3):315–22.
5. Gujar SK, Gandhi D. Congenital malformations of the orbit. Neuroimaging Clin N Am 2011;21(3):585–602, viii.
6. Barkovich A. Congenital malformations of the brain and skull. In: Barkovich A, editor. Pediatric neuroimaging. 4th edition. Philadelphia: Lippincott Williams and Wilkins; 2005. p. 291–405.
7. Fitzpatrick DR, van Heyningen V. Developmental eye disorders. Curr Opin Genet Dev 2005;15(3):348–53.
8. Bardakjian T, Weiss A, Schneider AS. Anophthalmia/microphthalmia overview. In: Pagon RA, Adam MP, Ardinger HH, et al, editors. GeneReviews® [Internet]. Seattle (WA): University of Washington; 1993–2015. Available at: http://www.ncbi.nlm.nih.gov/books/NBK1378/.
9. Schoenwolf G, Bleyl S, Brauer P, et al. Development of the eyes. In: Schoenwolf G, Bleyl S, Brauer P, et al, editors. Larsen's human embryology. 5th edition. Philadelphia: Churchill Livingstone Elsevier; 2015. p. 488–500.
10. Ito YA, Walter MA. Genomics and anterior segment dysgenesis: a review. Clin Experiment Ophthalmol 2014;42(1):13–24.
11. Kandpal H, Vashisht S, Sharma R, et al. Imaging spectrum of pediatric orbital pathology: a pictorial review. Indian J Ophthalmol 2006;54(4):227–36.
12. Kaufman LM, Villablanca JP, Mafee MF. Diagnostic imaging of cystic lesions in the child's orbit. Radiol Clin North Am 1998;36(6):1149–63, xi.
13. Gorospe L, Royo A, Berrocal T, et al. Imaging of orbital disorders in pediatric patients. Eur Radiol 2003;13(8):2012–26.
14. Castillo M, Mukherji SK, Wagle NS. Imaging of the pediatric orbit. Neuroimaging Clin N Am 2000;10(1):95–116, viii.
15. Levin AV. Congenital eye anomalies. Pediatr Clin North Am 2003;50(1):55–76.
16. Ellika S, Robson CD, Heidary G, et al. Morning glory disc anomaly: characteristic MR imaging findings. AJNR Am J Neuroradiol 2013;34(10):2010–4.
17. Quah BL, Hamilton J, Blaser S, et al. Morning glory disc anomaly, midline cranial defects and abnormal carotid circulation: an association worth looking for. Pediatr Radiol 2005;35(5):525–8.
18. Kindler P. Morning glory syndrome: unusual congenital optic disk anomaly. Am J Ophthalmol 1970;69(3):376–84.
19. Traboulsi EI. Morning glory disk anomaly – more than meets the eye. J AAPOS 2009;13(4):333–4.
20. Krishnan C, Roy A, Traboulsi E. Morning glory disk anomaly, choroidal coloboma, and congenital constrictive malformations of the internal carotid arteries (moyamoya disease). Ophthalmic Genet 2000;21(1):21–4.
21. Puvanachandra N, Heran MK, Lyons CJ. Morning glory disk anomaly with ipsilateral capillary hemangioma, agenesis of the internal carotid artery, and

Horner syndrome: a variant of PHACES syndrome? J AAPOS 2008;12(5):528–30.
22. Smirniotopoulos JG, Bargallo N, Mafee MF. Differential diagnosis of leukokoria: radiologic-pathologic correlation. Radiographics 1994;14(5):1059–79 [quiz: 1081–2].
23. Kaste SC, Jenkins JJ 3rd, Meyer D, et al. Persistent hyperplastic primary vitreous of the eye: imaging findings with pathologic correlation. AJR Am J Roentgenol 1994;162(2):437–40.
24. Galluzzi P, Venturi C, Cerase A, et al. Coats disease: smaller volume of the affected globe. Radiology 2001;221(1):64–9.
25. Parsa CF. Focal venous hypertension as a pathophysiologic mechanism for tissue hypertrophy, port-wine stains, the Sturge-Weber syndrome, and related disorders: proof of concept with novel hypothesis for underlying etiological cause (an American Ophthalmological Society thesis). Trans Am Ophthalmol Soc 2013;111:180–215.
26. Robertson DM. Ophthalmic manifestations of tuberous sclerosis. Ann N Y Acad Sci 1991;615:17–25.
27. Toy BC, Agron E, Nigam D, et al. Longitudinal analysis of retinal hemangioblastomatosis and visual function in ocular von Hippel-Lindau disease. Ophthalmology 2012;119(12):2622–30.
28. Wong WT, Chew EY. Ocular von Hippel-Lindau disease: clinical update and emerging treatments. Curr Opin Ophthalmol 2008;19(3):213–7.
29. Meyerle CB, Dahr SS, Wetjen NM, et al. Clinical course of retrobulbar hemangioblastomas in von Hippel-Lindau disease. Ophthalmology 2008; 115(8):1382–9.
30. Chew EY. Ocular manifestations of von Hippel-Lindau disease: clinical and genetic investigations. Trans Am Ophthalmol Soc 2005;103:495–511.
31. Parisi MA, Doherty D, Chance PF, et al. Joubert syndrome (and related disorders) (OMIM 213300). Eur J Hum Genet 2007;15(5):511–21.
32. Kava M, Chitayat D, Blaser S, et al. Eye and brain abnormalities in congenital muscular dystrophies caused by fukutin-related protein gene (FKRP) mutations. Pediatr Neurol 2013;49(5):374–8.
33. Fruhman G, Eble TN, Gambhir N, et al. Ophthalmologic findings in Aicardi syndrome. J AAPOS 2012; 16(3):238–41.
34. Shah PK, Narendran V, Kalpana N. Aicardi syndrome: the importance of an ophthalmologist in its diagnosis. Indian J Ophthalmol 2009;57(3):234–6.
35. Aicardi J. Aicardi syndrome. Brain Dev 2005;27(3): 164–71.
36. Entesarian M, Matsson H, Klar J, et al. Mutations in the gene encoding fibroblast growth factor 10 are associated with aplasia of lacrimal and salivary glands. Nat Genet 2005;37(2):125–7.
37. Inan UU, Yilmaz MD, Demir Y, et al. Characteristics of lacrimo-auriculo-dento-digital (LADD) syndrome: case report of a family and literature review. Int J Pediatr Otorhinolaryngol 2006;70(7):1307–14.
38. Graeber CP, Hunter DG, Engle EC. The genetic basis of incomitant strabismus: consolidation of the current knowledge of the genetic foundations of disease. Semin Ophthalmol 2013;28(5–6):427–37.
39. Bilaniuk LT, Farber M. Imaging of developmental anomalies of the eye and the orbit. AJNR Am J Neuroradiol 1992;13(2):793–803.
40. Mulliken JB, Glowacki J. Hemangiomas and vascular malformations in infants and children: a classification based on endothelial characteristics. Plast Reconstr Surg 1982;69(3):412–22.
41. Katz SE, Rootman J, Vangveeravong S, et al. Combined venous lymphatic malformations of the orbit (so-called lymphangiomas). Association with noncontiguous intracranial vascular anomalies. Ophthalmology 1998;105(1):176–84.
42. Bisdorff A, Mulliken JB, Carrico J, et al. Intracranial vascular anomalies in patients with periorbital lymphatic and lymphaticovenous malformations. AJNR Am J Neuroradiol 2007;28(2):335–41.
43. Chung EM, Smirniotopoulos JG, Specht CS, et al. From the archives of the AFIP: pediatric orbit tumors and tumorlike lesions: nonosseous lesions of the extraocular orbit. Radiographics 2007;27(6):1777–99.
44. Barnes PD, Robson CD, Robertson RL, et al. Pediatric orbital and visual pathway lesions. Neuroimaging Clin N Am 1996;6(1):179–98.
45. Kurul S, Cakmakci H, Kovanlikaya A, et al. The benign course of carotid-cavernous fistula in a child. Eur J Radiol 2001;39(2):77–9.
46. Lau FH, Yuen HK, Rao SK, et al. Spontaneous carotid cavernous fistula in a pediatric patient: case report and review of literature. J AAPOS 2005;9(3): 292–4.
47. Gossman MD, Berlin AJ, Weinstein MA, et al. Spontaneous direct carotid-cavernous fistula in childhood. Ophthal Plast Reconstr Surg 1993;9(1): 62–5.
48. Hollands JK, Santarius T, Kirkpatrick PJ, et al. Treatment of a direct carotid-cavernous fistula in a patient with type IV Ehlers-Danlos syndrome: a novel approach. Neuroradiology 2006;48(7):491–4.
49. Burrows PE, Laor T, Paltiel H, et al. Diagnostic imaging in the evaluation of vascular birthmarks. Dermatol Clin 1998;16(3):455–88.
50. Shields CL, Shields JA, Honavar SG, et al. Primary ophthalmic rhabdomyosarcoma in 33 patients. Trans Am Ophthalmol Soc 2001;99:133–42.
51. Shields CL, Shields JA, Honavar SG, et al. Clinical spectrum of primary ophthalmic rhabdomyosarcoma. Ophthalmology 2001;108(12):2284–92.
52. Crist WM, Anderson JR, Meza JL, et al. Intergroup rhabdomyosarcoma study-IV: results for patients with nonmetastatic disease. J Clin Oncol 2001; 19(12):3091–102.

53. Rao AA, Naheedy JH, Chen JY, et al. A clinical update and radiologic review of pediatric orbital and ocular tumors. J Oncol 2013;2013:975908.
54. Huh WW, Fitzgerald N, Mahajan A, et al. Pediatric sarcomas and related tumors of the head and neck. Cancer Treat Rev 2011;37(6):431–9.
55. Huh WW, Mahajan A. Ophthalmic oncology. In: Esmaeli B, editor. Ophthalmic oncology. Boston (MA): Springer; 2011. p. 61–7.
56. Shields JA, Shields CL. Rhabdomyosarcoma: review for the ophthalmologist. Surv Ophthalmol 2003; 48(1):39–57.
57. Vosoghi H, Rodriguez-Galindo C, Wilson MW. Orbital involvement in Langerhans cell histiocytosis. Ophthal Plast Reconstr Surg 2009;25(6):430–3.
58. Banna M, Aur R, Akkad S. Orbital granulocytic sarcoma. AJNR Am J Neuroradiol 1991;12(2):255–8.
59. Valvassori GE, Sabnis SS, Mafee RF, et al. Imaging of orbital lymphoproliferative disorders. Radiol Clin North Am 1999;37(1):135–50, x–xi.
60. D'Ambrosio N, Lyo J, Young R, et al. Common and unusual craniofacial manifestations of metastatic neuroblastoma. Neuroradiology 2010;52(6):549–53.
61. D'Ambrosio N, Lyo JK, Young RJ, et al. Imaging of metastatic CNS neuroblastoma. AJR Am J Roentgenol 2010;194(5):1223–9.
62. Chung EM, Specht CS, Schroeder JW. From the archives of the AFIP: pediatric orbit tumors and tumor-like lesions: neuroepithelial lesions of the ocular globe and optic nerve. Radiographics 2007;27(4): 1159–86.
63. Dimaras H, Kimani K, Dimba EA, et al. Retinoblastoma. Lancet 2012;379(9824):1436–46.
64. LaRocca V, Gorelick G, Kaufman LM. Medical imaging in pediatric neuro-ophthalmology. Neuroimaging Clin N Am 2005;15(1):85–105.
65. Passi N, Degnan AJ, Levy LM. MR imaging of papilledema and visual pathways: effects of increased intracranial pressure and pathophysiologic mechanisms. AJNR Am J Neuroradiol 2013;34(5):919–24.